FLUX AND SPECTRUM OF NEUTRONS GENERATED FROM 25 MV MEDICAL X-RAY THERAPY MACHINE

THESIS

Mark J. Rossano
Lieutenant, USN

AFIT/GNE/ENP/89J-1

DEPARTMENT OF THE AIR FORCE
AIR UNIVERSITY
AIR FORCE INSTITUTE OF TECHNOLOGY

Wright-Patterson Air Force Base, Ohio

FLUX AND SPECTRUM OF NEUTRONS GENERATED FROM 25 MV MEDICAL X-RAY THERAPY MACHINE

THESIS

Mark J. Rossano
Lieutenant, USN

AFIT/GNE/ENP/89J-1

Approved for public release: distribution unlimited

AFIT/GNE/ENP/89J-1

FLUX AND SPECTRUM OF NEUTRONS GENERATED FROM 25 MV MEDICAL X-RAY THERAPY MACHINE

THESIS

Presented to the Faculty of the School of Engineering

of the Air Force Institute of Technology

Air University

In Partial Fulfillment of the

Requirements for the Degree of

Master of Science in Nuclear Science

Mark J. Rossano

Lieutenant, USN

May, 1989

Preface

The purpose of this study was to develop procedures for monitoring neutron radiation emitted by a high-energy x-ray therapy machine installed at Wright-Patterson Air Force Base Medical Center. With this procedure hospital personnel may record the inevitable non-therapeutic patient neutron dose in rem. In addition, significant changes in monitoring results may give an indication to operators that the equipment requires corrective maintenance.

In order to make the desired neutron dose measurements, the thin foil activation method was employed using gold as the foil material. Activation of gold by neutrons, and subsequent beta decay was measured with two types of counting system. By using neutron moderators of two types, a system was calibrated with which fluence may be determined conveniently by operators every time the x-ray machine is used, and the neutron energy spectrum verified periodically by more skilled radiation monitoring personnel.

The detection methods were tested extensively using three Pu-Be neutron sources of known output under controlled conditions. A single set of irradiations was completed under hospital conditions using a BBC 45-MeV betatron. Based on all results, the repeatability of the techniques employed was demonstrated, although the inherent accuracy of spectrum determination could not be verified. This is a consequence of the fact that all of the neutron sources with a known spectrum were essentially identical, and the results of the method are known to be highly dependent on the experimenter's initial knowledge of the neutron spectrum.

In performing the experimentation and writing this thesis I have had a great deal of help from others. I am deeply indebted to my faculty advisor, Dr. George John for his continuing patience and guidance. I also wish to thank Lt. Col. John Swanson of Wright-Patterson

Air Force Base Medical Center, Dr. Don Ruegsegger of Miami Valley Hospital, Dr. Richard McCall of Stanford University Linear Accelerator Center and Mr. Robert Hendricks of the AFIT Physics Laboratory for their consultation and assistance during the experimental stages of the thesis. A word of thanks is also owed to Joe Hoefele and Jack Tiffany of the AFIT Model Fabrication Shop for their cooperation in building the necessary hardware. Finally, I wish to thank my wife Martha for her support, assistance, and understanding throughout this effort, without which I am certain this study could never have come to completion.

Mark J. Rossano

Contents

List of Figures

List of Tables

Abstract

A procedure was developed for the routine monitoring of neutron dose absorbed by patients receiving x-ray therapy with high-energy electron accelerators. The source of the neutrons was photonuclear reactions. The detection system used to measure them is described.

Three methods are described and compared for measuring the neutron flux by activation of thin gold foils. These included the cadmium-difference method for thermal flux determination, a cadmium-clad polyethylene moderator known to have a relatively "flat" response to neutrons in the energy range of interest, and a Bonner sphere set for measuring flux and the neutron energy spectrum. Results in an actual hospital installation using a BBC 45-MeV betatron revealed whole body neutron dose rates of approximately 1.5 mrem per photon rad. Two beta counting systems were calibrated so that routine measurements of neutron dose could be estimated from foil activation data and monitored for unexpected changes.

FLUX AND SPECTRUM OF NEUTRONS GENERATED FROM 25 MV MEDICAL X-RAY THERAPY MACHINE

I. Introduction

For over forty years electron accelerators have been used to provide energetic x-ray beams for radiation oncology (1:2). When beam energies exceed 10 MeV photonuclear reactions produce a significant number of neutrons. These neutrons are undesirable because they expose the patient's entire body rather than just the treatment site. Consequently, it is important to monitor the neutrons either periodically or routinely to ensure that the whole body neutron dose remains an inconsequential fraction of the therapeutic dose. Such routine monitoring requires the implementation of a simple and reproducible method for measuring neutron fluence. With knowledge of the fluence, dose can then be calculated. The method must also be capable of measuring a low level of neutrons in the presence of a high x-ray flux.

The detection of low neutron fluences accompanied by the large x-ray flux present in the treatment room requires a detector that is insensitive to the x-rays. Real time detectors such as proportional counters, scintillators or semiconductor detectors are unusable because the high x-ray flux would saturate them. One suitable detection method is the activation of a material with a high neutron absorption cross-section and a low cross-section for photonuclear reactions. Gold is one such material. The characteristics which favor its use are that it has one stable isotope, ^{197}Au; its cross-section for producing ^{198}Au is 98.7 barns at 2200 m/s, the most probable speed for a thermal neutron at 20° C (2:41); the half-life of ^{198}Au is 2.69 days; each ^{198}Au decays by

emission of a beta particle; and it has a small cross-section for photonuclear reactions (3). For these reasons gold foil activation was selected for the neutron monitoring. With a half life of 2.69 days for the ^{198}Au activation product, neutron fluence can be integrated accurately even when the treatment session is interrupted over the course of minutes or hours. Also, this half life is sufficiently long to allow the foils to be counted at the end of each day with less than a 15% loss in beta activity because of the delay. When a flux integrator of the type used in this study has been calibrated, a simple multiplicative constant allows the counts to be used directly to estimate neutron fluence and dose.

In order to devise a neutron measurement system for hospital use, several steps were taken to calibrate the detectors and prove the usefulness of the methods described. First, two beta counting systems were constructed and their reliabilities verified. The counters were then calibrated for use with activated gold foils. This was done so that the saturation activity of the foils could be calculated from the counts recorded. Further, the anisotropy characteristics of a Pu-Be neutron source of known strength were measured so that flux could be estimated accurately at any position with respect to this source. A flux integrator system, using a polyethylene cylinder covered with cadmium and holding a gold foil at its center, was calibrated so that a constant factor describes the proportionality between irradiating flux and foil saturation activity. A Bonner sphere set, with gold foil detectors, was exposed under the same conditions as the flux integrators. This aided in the selection of a useful algorithm for deconvoluting neutron energy spectra. Finally, all three flux measurement techniques (Cd-difference pairs, flux integrators, Bonner spheres) were tested in a hospital environment. The hospital results are compared with the more rigidly controlled procedures of the AFIT laboratory.

The two beta detectors used include a windowless 2π gas-flow proportional counter and a thin window G-M "pancake" detector, both with standard timer and scaler modules. The initial setup utilized conventional methods to find the beta counting plateaus and verify system stability. Detector calibration involved the determination of six foil counting corrections, some of which are thickness dependent. This was accomplished by reducing the data from many irradiations of foils with varying thickness after exposing them to the same flux. Once the six foil thickness corrections were determined, counts obtained with a beta detector were converted to a thickness-independent saturation activity which is proportional to flux for any given neutron energy spectrum.

When the corrected foil saturation activity is calculated, it is possible to find a calibration factor for the flux integrator. A Pu-Be source of known strength was used to provide a standard flux for this calibration. A series of tests were made to investigate the anisotropy of neutron emission from this source so that flux could be estimated at any position with respect to the source. The flux integrator was then calibrated by using the source under conditions of low and high ground-plane-scattering.

Two foil sets were activated in Bonner spheres under condition similar to those for the flux integrator calibration. This was done to aid in selecting the best of three unfolding algorithms. After making this choice, all three foil activation techniques were used to monitor neutron production by Miami Valley Hospital's 45-MeV BBC Betatron. This unit is representative of such x-ray therapy devices. As such, it provided a prototypical environment for the development of neutron measurement techniques to be used later at Wright-Patterson AFB Medical Center. From the experimental data, fluence estimates were made and the results of the different activation methods compared.

The following sections of this report develop the theory and methods used to test and evaluate the foil activation techniques used for

neutron monitoring. Chapter II describes the theories of foil activation and Bonner Sphere spectrometry along with several supporting topics. Chapter III is a description of the experimental apparatus used. Chapter IV recounts the experimental procedures followed along with the results obtained. Chapter V presents a group of conclusions based on the experimental results, and recommendations for further refinement of the procedures used.

II. Theory

Photoneutron Production in Medical Electron Accelerators

Medical use of high-energy electron accelerators has permitted the application of energetic electron and x-ray beams for radiation oncology. With beam energies in the 10-MeV to 45-MeV range, the production of neutrons by photonuclear (γ,n) reactions can be significant. While it is possible for high-energy electrons to directly induce the emission of neutrons from a target nucleus, it is approximately 100 times more likely that photons of the same energy would produce such an emission (1:14). For this reason only the physics of photonuclear interactions is treated.

Electron accelerators for medical applications normally allow a choice of either an electron or an x-ray beam. In the x-ray mode energetic electrons are directed at a target of some high atomic number material, such as platinum, tungsten, or copper (2:131). The bremsstrahlung radiation produced when the electron beam strikes the metal target is collimated and aimed at the treatment site. The x ray spectrum includes photon energies up to that of the incident electron beam. Neutron production is governed by the properties of the giant resonance for photonuclear interactions in the particular target material. So long as the photon energy exceeds the neutron separation energy for the target nucleus, there exists a finite probability of neutron emission for targets of more than infinitesimal thickness.

Since all target materials and collimators in use are thick in terms of the electron range, some photonuclear reactions must take place. The (γ,n) separation energies for typical target materials range from 6.11 MeV for ^{195}Pt to 10.85 MeV for ^{63}Cu (1:20). Photoneutron cross sections peak in the 13 to 18 MeV range, with the peaks tending toward lower energies with increasing mass number (1:10-12). Since the

average energy of a Bremsstrahlung spectrum is about one third the energy of the incident electrons, many photoneutrons will be produced by electron accelerators operating at 25 MeV to 45 MeV. Experimental values of neutron fluence per rad of x rays used in treatment range from 3.2×10^3 $^{\dagger}_{0}n/cm^2$-rad up to 1.9×10^5 $^{\dagger}_{0}n/cm^2$-rad for commercially available machines (1:96).

Neutron Detection by Activation of Thin Foils

The relations needed for calculating foil activity caused by neutron absorption are presented in this section. They are well known and presented in detail in many textbooks on radiation detection. They are repeated here to identify the quantities needed for the determination of fluence, the assumptions made, and possible sources of error.

The reaction rate for activation of a material with N_T absorbers is given by the relation (4:36):

$$R = N_T \int_0^{\infty} \sigma_a(v) n(v) v \, dv \qquad (1)$$

where

R is the formation rate of the product nuclide per unit volume [cm^{-3}-s^{-1}]

N_T is the number of target nuclei per unit volume [cm^{-3}]

$\sigma_a(v)$ is energy-dependent neutron absorption microscopic cross section for the target nuclide [cm^2]

$n(v)$ is number of neutrons per unit volume as a function of speed [$^{\dagger}_{0}n/cm^3$]

v is neutron speed [cm/s].

In order to calculate the reaction rate it is clear that we must know the spectrum of neutrons and the absorption cross section. However, if the cross section for the absorber varies as 1/v it is possible

to divide this integral into two regions, one for the 1/v dependence, and the other for all other reactions. If we have a 1/v absorber and there are no resonances, it is true that:

$$\sigma_{a0} v_0 = \sigma_a(v) v \tag{2}$$

where

v_0 is the most probable speed of a neutron for a Maxwell-Boltzmann distribution at 293.15 K

σ_{a0} is the microscopic neutron absorption cross section at v_0.

By using this relation in equation (1) the integration is possible over the range of neutron speeds where the 1/v dependence applies. For a strict 1/v dependence this is represented in the following solution for reaction rate:

$$\begin{aligned} R &= N_T \int_0^\infty \frac{\sigma_{a0} v_0}{v} n(v) v \, dv \\ &= N_T \sigma_{a0} v_0 \int_0^\infty n(v) \, dv \\ &= N_T \sigma_{a0} (n_0 v_0) \\ R &= N_T \sigma_{a0} \phi_0 \end{aligned} \tag{3}$$

where

$\phi_0 = n_0 v_0$, the total neutron flux [$\frac{1}{0}$n/cm^2-s]

n_0 is the number of neutrons of all speeds, per unit volume.

If the product nuclide is unstable with a known decay constant, its disintegration rate will be described by the differential equation:

$$\frac{dN(t_e)}{dt} = R - \lambda N(t_e) \tag{4}$$

where

$N(t_e)$ is the number of product nuclei per unit volume after an irradiation of t_e seconds

λ is the product nuclide decay constant $[s^{-1}]$.

As t_e approaches infinity, the target activity will approach a constant such that the reaction and decay rates are equal. This is the saturation activity, $A_s = A(t_e = \infty)$ $[s^{-1}\text{-}cm^{-3}]$. A_s may be calculated from a measurement of absorber activity after irradiation, so it provides a convenient way to determine R, which can be used directly to calculate flux. This is clear in the following relation which expresses R in terms of A.

$$R = A_s = A(t_e)/(1 - e^{-\lambda t_e}) \tag{5}$$

A useful property of many materials, gold and indium among them, is that for thermal neutron energies ($E \leq 0.5$ev), $\sigma_a(v)$ is proportional to 1/v. However, there are resonances above 0.5 eV that add to the activation expected from the 1/v character of σ. Consequently, this resonance response must be included in the equation for A_s by partitioning the integral between the thermal and epithermal regions as follows:

$$\begin{aligned} A_s &= N_T\left[\int_{thermal} \frac{\sigma_{a0} v_0}{v} n(v)\, v\, dv + \int_{epithermal} \sigma_a(v)\, n(v)\, v\, dv\right] \\ &= N_T\left[\sigma_{a0} v_0 n_{thermal} + \int_{epithermal} \sigma_a(v)\, n(v)\, v\, dv\right] \end{aligned} \tag{6}$$

where

σ_{a0} is defined as the microscopic neutron absorption cross-section at 2200 m/s, the most probable speed of a neutron for a Maxwell-Boltzmann distribution at 293.15 K.

Saturation activity is represented as having contributions from thermal and epithermal neutrons so that flux can be calculated. Use of the cadmium-difference method and tabulated values of the resonance integral allows this to be done.

The saturation activity can be calculated from the counts obtained in a counting time of t_c, with the count started at an elapsed time of t_w from the end of the irradiation period, t_e. This relation is given in equation (7) (5:5), with a complete derivation found in Appendix A.

$$A_s' = \frac{\lambda[C(t_c) - C_{BC}]e^{\lambda t_w}}{\epsilon(1 - e^{-\lambda t_c})(1 - e^{-\lambda t_e})} \tag{7}$$

where

A_s' is the calculated saturation activity that is induced when self-shielding is present

$C(t_c)$ is recorded detector counts in time t_c

C_{BC} is background counts in time t_c

ϵ is the detector counting efficiency.

The value of A_s' obtained with equation (7) must be corrected for neutron self-shielding of foils before it can be used in equation (6) to calculate the flux. For this, a correction factor is needed to calculate the activity that would have been produced had no self-shielding occurred. Thus:

$$A_s = A_s'/\alpha(x) \tag{8}$$

where

$\alpha(x)$ is an experimentally determined correction factor for self-shielding of neutrons by the foil

x is foil thickness.

Together, equations (6) and (7) form the basis for determining neutron flux by foil activation. The cadmium-difference method is one of the most useful foil activation methods because it permits the calculation of thermal flux absolutely without directly measuring the epithermal flux contribution to A_s.

Cd-Difference Method for Thermal Neutron Flux Determination

In the previous section, equations (6) and (7) established a relationship between measured foil activity and flux. By itself, this connection is not useful because an analytic solution from one foil activation requires prior knowledge of $\sigma_a(\epsilon)$ and $n(\epsilon)$ for epithermal energies. In general $\sigma_a(\epsilon)$ will be known but $n(\epsilon)$ will not. With <u>two</u> foils, a solution is possible by taking advantage of the fact that cadmium acts as a thermal neutron "filter". Natural cadmium has a very large absorption cross section for thermal neutrons (σ_{a0} = 2400 barns) which drops rapidly to 5 barns at 5.0 eV, thereafter remaining nearly constant (4:36). This property allows us to determine the "resonance integral" for neutron absorption by irradiating a pair of foils in the same flux with one foil bare and the other covered with cadmium. This is known as a cadmium-difference pair. Further, the Cd-difference method makes it possible to calculate the portion of the activity induced in a bare foil by epithermal neutrons without actually knowing what the epithermal flux was.

If a Cd-difference pair is irradiated, the bare foil will be activated as a function of $\phi(\epsilon)$ at all energies, while the covered foil will be activated by essentially resonance absorption of epithermal neutrons alone. The difference between the activity of the bare foil and the covered foil is the activity produced principally by the thermal flux. For this reason, Equation (6) may be recast in the following form:

$$A_s = A_{st} + N_T \int_{0.5eV}^{\infty} \sigma_a(E)\phi(E)dE$$

$$= A_{st} + A_{se}$$

$$= A_{st} + F_{Cd} A_s^{Cd}$$

$$A_{st} = A_s - F_{Cd} A_s^{Cd} \qquad (9)$$

where

A_{st} is the saturation activity per unit volume produced by neutrons with E < 0.5 eV

F_{Cd} is a correction factor for the absorption of epithermal neutrons by cadmium

A_s^{Cd} is the saturation activity per unit volume of the cadmium covered foil

$\sigma_a(E)$ is the microscopic neutron-absorption cross-section of the target as a function of energy

$\phi(E)$ is neutron flux per unit of energy as a function of energy.

F_{Cd} is usually found by experiment for various cadmium thicknesses, but may be calculated based on the total cross-section for cadmium in the resonance region, where it is nearly energy independent (5:23). There is also a small amount of thermal neutron leakage through the cadmium cover, but for Cd thicknesses greater than 0.38 mm this leakage is less than 0.1%, so it may be neglected (5:23). The significance of this derivation is that by using Equation (9), a Cd-difference pair yields the data needed to measure thermal flux when epithermal flux is unknown and need not otherwise be found. By solving for A_{st} the reaction rate due to thermal neutrons is determined. Equation (3) may then be recast in the form:

$$A_{st} = N_T \sigma_{a0} \phi_0$$

This equation is used with (8) and (9) to yield a relationship between flux and the saturation activities of two foils irradiated as a Cd-difference pair.

$$\phi_0 = \left(\frac{A_s'}{\alpha_1} - \frac{A_s'^{Cd}}{\alpha_2} F_{Cd} \right) / \sigma_{a0} N_T$$

where

α_1 is $\alpha(v)$ for the foil used to determine A_s'

α_2 is $\alpha(v)$ for the foil used to determine $A_s'^{Cd}$.

If A_s' is calculated per unit mass rather than volume this relation is stated as:

$$\phi_0 = A \left(\frac{A_s'}{\alpha_1} - \frac{A_s'^{Cd}}{\alpha_2} F_{Cd} \right) / \sigma_{a0} N_a$$

where

A is the atomic weight of the target nuclide

N_a is Avogadro's number.

More generally, we would like to find the total thermal flux, ϕ_{th}. This quantity is obtained from the relation:

$$\phi_{th} = 1.128 A \left(\frac{A_s'}{\alpha_1} - \frac{A_s'^{Cd}}{\alpha_2} F_{Cd} \right) / \sigma_{a0} N_a \qquad (10)$$

The constant factor, 1.128, is introduced to correct for the difference between the average and most probable speeds in a Maxwell-Boltzmann distribution.

Detector Counting Efficiency Factor

The determination of A_s from Equation (6) requires knowledge of the detector counting efficiency, ϵ. The efficiency is the product of six factors:

$$\epsilon = f_g f_w f_e f_\gamma(x) f_{bs}(x) f_s(x) \qquad (11)$$

where

f_g is detector geometry factor

f_w is detector window absorption factor

f_e is intrinsic beta counting efficiency

$f_\gamma(x)$ is gamma counting correction

$f_{bs}(x)$ is backscatter counting correction

$f_s(x)$ is foil self absorption and self scatter correction

x is foil thickness.

The factors in this equation apply to a source located outside a detector that has an entrance window. They are also meant for a source such as gold that emits a beta particle with each decay followed by a gamma ray for 99% of the decays. Thus, an absolute determination of efficiency requires that the counts caused by gammas be subtracted from the total count.

Of the six factors which make up ϵ, the first three are independent of foil thickness. The term f_g is normally assumed to be the solid angle subtended by the detector sensitive volume as measured from the foil center. The geometry factor for the 2π proportional flow counter used in this study is $f_g = 0.49$ (6:61). The G-M counter that was used for some of the counts has a geometry factor of $f_g = 0.38$ which is calculated in Appendix A. The window absorption factor is unity for the 2π counter because it is windowless. A thin window G-M counter does have a meaningful f_w, with $f_w < 1.0$. For all of the detector configurations $f_e = 1.0$ (7:59). The values for f_γ, f_{bs} and f_s for indium are taken from Greenfield et al. by using an exponential fit of the tabular data (6:58, 60).

The thickness-dependent counting corrections for gold were found

experimentally. In general, these corrections may be determined separately. The method is well known and described in detail by Price (4:132) and Greenfield (6). In practice these methods are very tedious. A simpler alternative is to find a single correction which is the product of all three factors. Greenfield describes the determination of this combined factor (6). Foils of many different thicknesses are irradiated in a constant flux. If the thinnest foils are nearly weightless (a few $\mu g/cm^2$ or less) an empirical relationship between thickness and activity can be deduced. When this relation is extrapolated to zero foil thickness the thickness dependence of count rate is described in absolute terms. The combined correction factor is therefore:

$$f_v(x)f_{bs}(x)f_s(x) = C_s(x)/C_s(0)\alpha(x)$$

where

C_s is the detector saturation count rate $[s^{-1}]$, $C_s = \epsilon A_s$.

If self shielding is negligible, the correction factor is more simply described by $C_s(x)/C_s(0)$.

The fabrication of extremely thin foils is not always feasible. An alternative calculation for $f_v f_{bs} f_s$ is possible if an initial assumption about the nature of the thickness dependence is made. The assumption used in this study is that for gold foil thicknesses in the range of 45 mg/cm^2 to 110 mg/cm^2, the dependence is exponential. This assumption is based on the fact that for foil thicknesses which are neither very thin nor thick in terms of the range of the beta particles emitted, each of the counting corrections has an approximately exponential dependence. The product of these factors will therefore be approximately exponential. Using indium as an example, Greenfield's data shows a nearly perfect correlation to an exponential function for the same three factor correction over a similar thickness range (6:58). Even though gold and indium do not have identical characteristics, the similarity in their

beta energies and electron ranges is such that this is a reasonable comparison. From this assumption, the combined factor may be expressed in the form:

$$f_v(x)f_{bs}(x)f_s(x) = ae^{-\mu x} \tag{12}$$

The factor "a" is an undetermined proportionality constant which accounts for the fact that it is unreasonable to extrapolate this function to zero foil thickness. The logic of this approach parallels Greenfield's method, albeit with somewhat reduced accuracy. From (12), equation (1) may be recast in the form:

$$C_s = ae^{-\mu x} f_g f_u f_e N_T \int_0^x \sigma_a(E)\phi(E)dE \tag{13}$$

If all of the constant and energy-dependent terms are gathered symbolically into one function, b(E), equation (13) may be expressed as:

$$C_s = b(E)e^{-\mu x} \tag{14}$$

The constant, a, cannot be factored from b(E) without solving the integral term. It is impractical to do so because the fast neutron spectrum in the graphite pile used for calibrations is not well known. A least-squares fit of irradiation data can therefore only determine b(E) for this unknown neutron spectrum, and μ. As long as self-shielding is insignificant, μ can be found for a given range of foil thicknesses. By finding the mean value of μ from several irradiations $f_v f_{bs} f_s$ is thereby determined to within the unknown constant, a. The constant, a, can then be found if foils are irradiated in a known thermal flux. The AFIT graphite pile has a well known thermal component (5). By recasting Equation (10) in terms of (12) the following relation is obtained:

$$\phi_{th} = 1.128 A\left(\frac{1}{a}\right)\left(\frac{C_s}{\alpha_1 f_g f_u f_e e^{-\mu x_1}} - \frac{C_s^{Cd}}{\alpha_2 f_g f_u f_e e^{-\mu x_2}} F_{Cd}\right) / \sigma_{a0} N_a \qquad (15)$$

where

C_s^{Cd} is the saturation count rate of the Cd covered foil

x_1 and x_2 are the thicknesses of the bare and Cd covered foils, respectively.

The constant a is the only unknown in Equation (12), so the irradiation of cadmium-difference pairs in several known thermal fluxes permits it to be calculated from a linear regression. Published sources contain $\alpha(x)$ for gold (7:34, 39) so all required counting corrections are available.

The Bonner Sphere Set as a Neutron Spectrometer

In 1960 it was suggested by Bramblett, et al. that a set of neutron moderating spheres of various sizes could be useful in determining neutron spectra. By placing a thermal neutron detector in the center of each sphere, a combination of the non-linear dependencies of moderation and absorption on sphere diameter results in a set of independent response functions for each sphere-detector combination (9:1-12). The response of a set of spheres may be characterized by the equation set:

$$A_{sj} = \int_{All\ E} \sigma_j(E)\phi(E)dE \quad ; \quad j = 1, 2, \ldots, M \qquad (16)$$

where

A_{sj} is the saturation activity of the j^{th} detector

$\sigma_j(E)$ is the response of the j^{th} detector as a function of energy

$\phi(E)$ is neutron flux

M is the total number of detectors.

Equation (16) is known as a Fredholm integral equation of the first kind. It may be solved analytically or numerically for $\phi(F)$ if $\sigma(E)$ is a set of analytic functions, but in general this is not the case. An approximate solution may still be obtained by replacing $\sigma(E)$ with a set of constant approximations over a finite number of energy intervals. By matrix methods a solution for ϕ is obtained which is an average for a given energy interval or "bin". The integral equation may now be replaced by the summation (9:2):

$$A_{sj} \approx \sum_{k=1}^{N} \sigma_{jk} \phi_k \tag{17}$$

where

σ_{jk} is the response of the j^{th} detector to the k^{th} energy bin

ϕ_k is the neutron flux averaged over the k^{th} energy bin

N is the total number of energy bins.

In matrix notation equation (17) is represented by:

$$\bar{A} = \underline{\sigma}\bar{\phi} \tag{18}$$

where

$\bar{A}$ is a vector of dimensions 1 x N

$\underline{\sigma}$ is a matrix of dimensions N x M

$\bar{\phi}$ is a vector of dimensions N x 1.

In principle, a solution for $\bar{\phi}$ is possible by solving the matrix equation:

$$\underline{\sigma}^{-1}\bar{A} = \bar{\phi} \tag{19}$$

In practice, enough energy bins are defined to describe adequately the neutron spectrum. However, the M detectors available are generally

insufficient to provide a unique solution for equation (19). Several computer codes have been written which attempt to deal with this ill-posed problem. An initial input for the shape of the spectrum (based on the physical conditions under which the neutrons are produced) is used as a start for determining the unfolded spectrum. A readily available and versatile example of such codes is BUNKI, developed by T. L. Johnson at the Naval Research Laboratory (10). The method used in BUNKI to solve for $\bar{\phi}$ is one where an initial guess for $\bar{\phi}$ is used in Equation (18) to solve for $\bar{A}$. BUNKI's calculated detector response is then compared with the actual (experimental) $\bar{A}$. The results of this comparison are used to perturb the original guess for $\bar{\phi}$ in such a way that the calculated $\bar{A}$ approaches the actual response. This cycle of perturbation and comparison is continued until $\bar{A}$(calculated) and $\bar{A}$(actual) agree within a prescribed error limit. When the fixed error criterion is met the program exits, returning the final $\bar{\phi}$ as its estimate for flux. In addition to meeting the error criterion, BUNKI allows the result to be smoothed to any initial spectrum. The method is described in detail by Johnson (11:4-6). The effect of this smoothing algorithm is to match the slope of the solution spectrum with that of the initial spectrum to within a specified amount for each energy bin.

Since the solution for the spectrum provided by BUNKI depends strongly on the validity of the initial spectrum input, a sound physical model for the initial guess is essential. Fortunately, the production of photoneutrons is sufficiently well understood to provide the general characteristics of the neutron spectra, so iterative recursion methods do provide a useful result.

General Characteristics of the Anticipated Spectra

The neutron spectra expected from medical electron accelerators have three energy components. The "virgin" spectrum from the apparatus resembles a fission spectrum with a similar average energy (on the order of 0.5 MeV to 2.0 MeV, depending on the target material and electron

beam energy (1:39, 40)). The measured spectrum is expected to contain two additional components as a consequence of scatter from the treatment facility surroundings. These scatter components include the characteristic "slowing down" spectrum where flux is proportional to 1/E, and a near Maxwell-Boltzmann distribution at thermal energies. The 1/E spectrum at intermediate energies is based simply on the physics of elastic scatter, which neutrons undergo in a moderator. The mechanics of this process are well known, and described in several references (11:24-28). The thermal distribution component results from the fact that after successive scatters, neutrons will nearly reach a thermal equilibrium with their surroundings, similar to ideal gas particles (11:66).

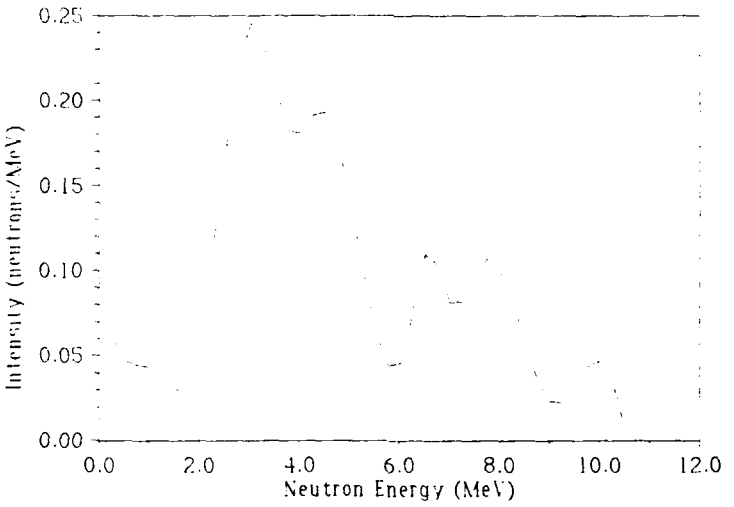

Figure 1. Plutonium-Beryllium Neutron Source Spectrum (12:176)

The spectrum from a photoneutron source will be the superposition of the three described components. The relative magnitudes of these components depend mostly on how much moderation versus absorption actually takes place. For the Pu-Be sources used in some of the calibration experiments the expected spectra are similar, with the major differences seen in the high-energy "virgin" component. Examples of both types of fast spectra are depicted in figures 1 and 2. For a Pu-Be

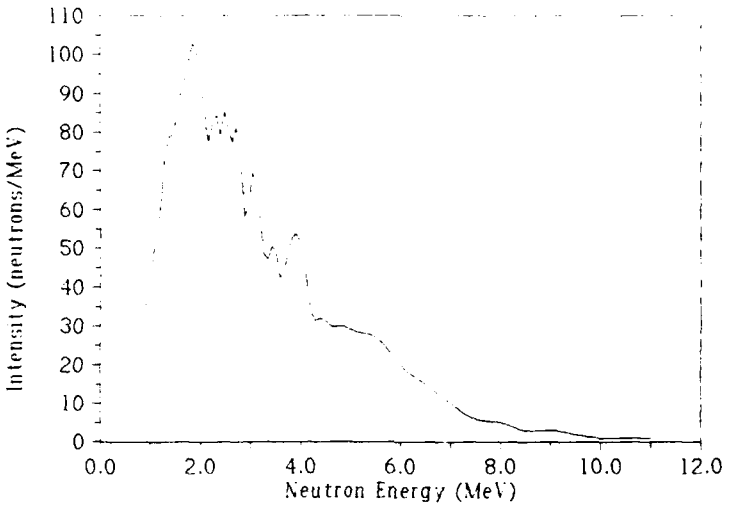

Figure 2. Lead Photoneutron Spectrum from a 31-MeV Electron Source (1:30)

source the average neutron energy is approximately 4.2 MeV, rather than the 0.5-MeV to 2.0-MeV average energy for fission and photoneutrons. In addition, Pu-Be sources have characteristic peaks at several energies due to a variety of resonances in both plutonium and beryllium.

Integrated Fluence and Dose Measurement

The Bonner sphere neutron spectrometer described previously has its greatest value in its ability to describe neutron production in terms of energy distribution as well as integral flux and fluence. This is desirable because the quality factor for neutrons varies widely over the energy range of interest. Table I, taken from NCRP 38 shows the energy dependence of quality factor.[1]

Once the spectrum of a neutron source has been determined, it is possible to simplify the monitoring of neutron fluence and dose. Several authors have described detectors exhibiting a response which is

1 It should be noted that a more recent report, NCRP 91, has recommended a doubling of the quality factors contained in Table I. The new values, now denoted by the symbol $\tilde{Q}$ may be adopted for general use in the near future.

TABLE I

Neutron Average Quality Factor at Energies Up To 14 MeV (13:21)

Neutron Energy [MeV]	$\overline{QF}$
Thermal	2
1×10^{-7}	2
1×10^{-6}	2
1×10^{-5}	2
1×10^{-4}	2
1×10^{-3}	2
1×10^{-2}	2.5
1×10^{-1}	7.5
1.0	11
2.5	9
5	8
7	7
10	6.5
14	7.5

approximately proportional to flux in the energy range 0.5 eV to 20 MeV. One of the most thorough investigations of such a detector was conducted by Bruninx (14). In experiments using indium foils and a 6" sphere made of paraffin, the ratio of flux to foil activity varied by a factor of 1.9 for a spectrum average energy which varied by a factor of 9.0 (14:662). McCall has stated that the response of a similar detector (the 6" x 6" Cd covered polyethylene cylinders described in subsequent sections) varies less than 10% for the kind of spectra encountered with medical electron accelerators (15). If a neutron source with a known

strength is used, calibration is possible with a simple linear fit of flux versus A_s. A linear regression can be used to determine K(E) in the relation (14:658):

$$A_s = \phi_{epithermal}/K(E) \tag{20}$$

where

K(E) is a calibration factor which varies slowly with neutron average energy.

By using the neutron spectrum estimated with Bonner Spheres an overall average quality factor can be calculated from Table I. A_s For a foil irradiated in the flux integrator may be directly related to dose equivalent from the widely published values for neutron linear energy transfer in tissue. The relation used by Johnson in his BUNKI code is (10):

$$H = \overline{QF}(\overline{LET}_{max}/d)\Phi \tag{21}$$

where

H is dose equivalent [rem]

Φ is neutron fluence = $tA_s/K(E)$

$\overline{LET}_{max}$ is the flux averaged maximum linear energy transfer in tissue

$\overline{QF}$ is flux averaged quality factor

d is tissue density ($d \approx 1.0$ g/cm^3).

III. Experimental Apparatus

To calibrate a neutron detection system and determine suitable procedures for its use, a variety of equipment and materials were employed. These items included:

- Detection foils and equipment used in their fabrication and handling
- Encapsulated Pu-Be neutron sources
- Neutron moderators used with the detection foils
- AFIT standard graphite pile (used for calibration)
- Miami Valley Hospital's BBC Asklepitron 45 (a 45-MeV Betatron)
- Beta radiation detectors used to count induced foil activity
- A rigid hanger used to suspend neutron sources and foils
- DEC VAX 11/780 Computer (for data reduction)
- Zenith Z-386 Desktop Computer (for data reduction)

Detection Foils

A total of seventy-seven circular foils were used in the experiments. Sixty-eight of these were assayed by the supplier to be 99.99% pure gold. Nine indium foils of natural isotropic composition (^{115}In - 95.7%, ^{113}In - 4.3%) were also used. These foils were assayed by the supplier to be 99.97% pure indium.

The gold foils were cut from sheet stock with hand punches. The punch diameters and sheet thicknesses (reported by the supplier) are listed below:

Punch Diameters [in]	Thicknesses [in]
7/16	0.002
1/2	0.0005
1/2	0.001
1/2	0.002
1	0.0005
1	0.001
1	0.002

All of the indium foils were cut with a 1" diameter punch from sheet reported by the supplier to be 0.002" thick.

All foils were inspected to ensure that they were cleanly cut. This was done to reduce the error in measuring foil diameter. No attempt was made to precisely match the thicknesses of foils. Once cut, the diameters of all foils were measured by placing them on the observation stage of a vertically mounted traveling microscope. This unit had a vernier scale for linear travel with a resolution of 0.001 cm. Its precision was estimated by repetitive measurements of a few of the foils to be within 0.002 cm. Foil weights, which varied between 31.2 mg and 501.8 mg were determined within 0.1 milligram using an analytical balance. The precision of this balance was estimated by repetitive measurements to be 0.2%. Prior to use each foil was washed with pure isopropanol and handled with clean tweezers. Between uses, foils were stored in separate polyethylene envelopes.

Some of the foils were irradiated with cadmium covers. These covers were all 25 mm in diameter. The cadmium covers were measured with a micrometer and found to have a range of thicknesses from 0.70 mm to 0.86 mm.

Encapsulated Pu-Be Neutron Sources

Three Pu-Be neutron sources were used for the foil irradiation experiments. Two of these are in the custody of AFIT, while one belongs to Stanford Linear Accelerator Center (SLAC). The AFIT sources were both ^{239}Pu-Be sources manufactured by Mound Laboratory. The source used for calibration of the Bonner sphere set and the 6" flux integrators described subsequently was serial number M1170. The second AFIT source, serial number M580, was used for a set of calibration irradiations in the AFIT standard graphite pile. The anisotropy of neutron emission for source M1170 was investigated so that flux could be calculated at various locations with respect to it. The anisotropy was found to be greater than that reported by Mound Laboratory. This increase suggests

that the source has elongated over time (12:175). A third source was used for irradiation of three gold foils. It is a ^{238}Pu-Be source belonging to SLAC. These foils were irradiated by R. C. McCall at SLAC and returned to AFIT for counting. The present day strength of all three sources is calculated in Appendix B. These strengths are:

M1170 - 1.10×10^7 $^{\frac{1}{0}}$n/s (October, 1986)

M580 - 1.05×10^7 $^{\frac{1}{0}}$n/s (October, 1986)

SLAC - 1.92×10^7 $^{\frac{1}{0}}$n/s (November, 1986)

Source M1170 has an anisotropy factor of $i(90^\circ) = 1.15$ where $i(\Theta)$ is the ratio of $\phi(\Theta)$ to ϕ(average) and Θ is the orientation angle with respect to the source long axis. The magnitude of $i(90^\circ)$is calculated from experimental data in Appendix C. For the SLAC source, McCall reports that $i(90^\circ) = 1.095$.

Neutron Moderators

Two types of moderators were fabricated for use with the detector foils. All were made of high density polyethylene, with a density of 0.95 g/cm^3. A set of four matched cylinders was made with a diameter of 150 cm and a height of 150 cm. These are covered with 0.50-mm thick, pure cadmium sheet, formed to shape, soldered at the seams, and attached to the exteriors of the cylinders with epoxy. A well of 50-mm diameter and 75-mm depth was bored in each cylinder. A polyethylene plug of matching dimensions with a cadmium disk affixed to one end was made to fill this hole. Foils were placed in the bottom of the well thus formed when irradiated, thereby encasing them in essentially solid polyethylene. Figure 3 is a phantom view of one of these "flux integrators".

The Bonner sphere set consists of six high density polyethylene spheres. Four of these were purchased from Ludlum Instruments, while the two largest were fabricated in the AFIT Model Shop. The sphere sizes were 2", 3", 5", 8", 10", and 12". All were bored radially with a

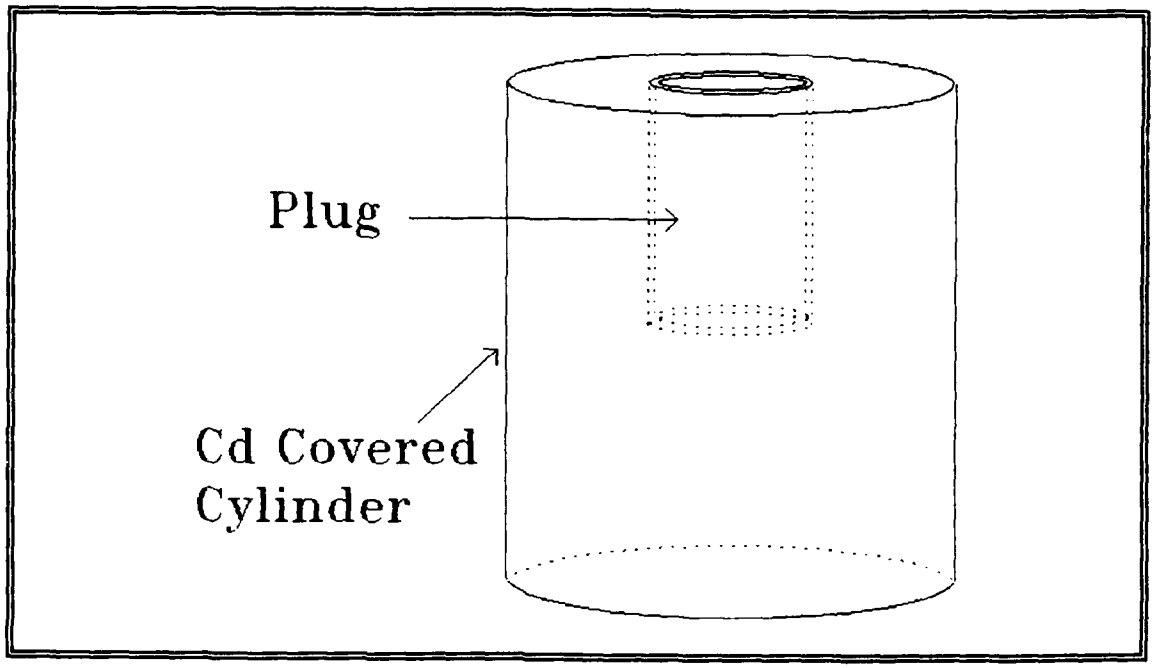

Figure 3. Flux Integrator Phantom View

5/8" diameter hole to 1/8" beyond center to allow a foil to be inserted at the center. Each was fitted with a plug of matching dimensions and material to fill this hole.

AFIT Standard Graphite Pile

The standard graphite pile at AFIT was used for several calibration irradiations of gold foils. This assembly is constructed of reactor grade graphite beams (AGOT). It is assembled from 18 crossed layers of graphite parallelepipeds (4" x 4" x 50") such that each layer is 4" thick, 48" wide, and 50" long. The assembled pile is covered on all six sides by 0.8-mm thick cadmium sheet which serves to prevent the escape of thermal neutrons while also preventing the entry of thermal neutrons from outside the pile (5:9).

The neutron source used with this pile (M580) fits in a recess cut for it in a movable element of the pile. This recess is 35.6 cm above the bottom plane of the pile and at the center of a horizontal plane. Foils were irradiated in each of the graphite stringers, FS1 through

FS9. Table II shows the distance between the source and foils for each of the stringers. Negative distances identify stringers which are located below the neutron source. A detailed description of the pile assembly is contained in reference 5.

TABLE II

Source-to-Foil Distance for Each Stringer

In the AFIT Standard Graphite Pile

Stringer Number	Foil Height [cm]
FS1	-26.7
FS2	-6.4
FS3	14.0
FS4	34.3
FS5	54.6
FS6	74.9
FS7	95.2
FS8	115.5
FS9	135.8

Miami Valley Hospital Betatron

A group of foils was irradiated with neutrons from a 45-MeV betatron used for cancer therapy with electron beams and high-energy x rays. The unit is a Brown-Boveri Asklepitron 45 installed at Miami Valley Hospital in Dayton, Ohio. This machine generates 45-MeV monoenergetic electrons in the betatron section. The beam is directed at a 2.0-mm thick platinum target to produce bremsstrahlung x rays. These x rays pass through a lead flattening filter and are collimated by a set of fixed and movable lead and tungsten shields (16:131). This arrangement, representative of many such machines, is depicted in Figure 4.

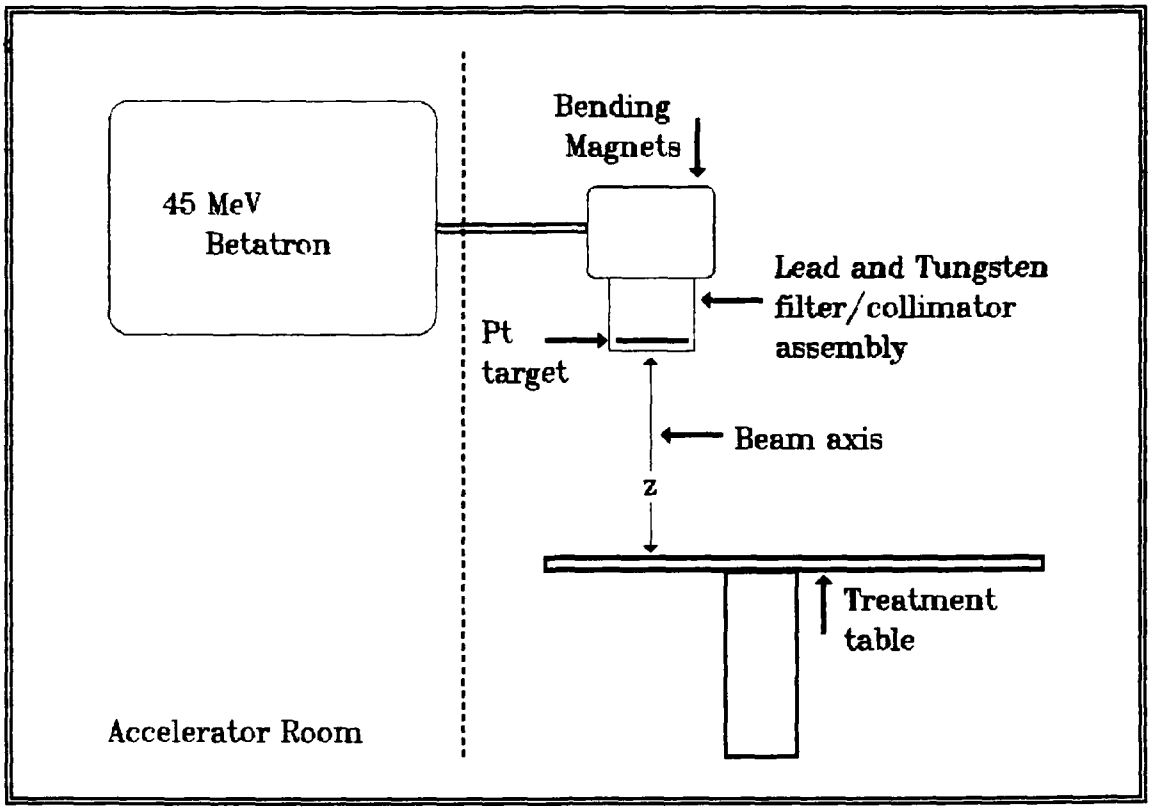

Figure 4. Betatron Treatment Facility Diagram

The photon beam from this machine interacts with the platinum target, flattening filter, and collimators to produce neutrons by photonuclear reactions.

The manufacturer of this machine specifies that with collimators in place, the photon dose rate is constant within the limits of the beam collimation area. At 1 cm outside the collimation area the photon dose is less than one percent of the maximum for a measurement plane 110 cm below the Pt target. In this same plane the photon dose rate drops to less than one tenth of a percent of the maximum at a distance of 10 cm from the edge of the collimated beam. The machine console is calibrated in "impulse units". The magnitude of impulse units equals the magnitude of photon dose in Rads (tissue) for a plane 110 cm below the Pt target. The photon beam intensity is reported to vary as $1/z^2$ where z is the distance from the target to the measurement plane (16).

Beta Radiation Detectors

To measure the foil beta activity induced by neutrons, two counting systems were assembled. One system uses a windowless gas flow proportional counter while the other uses a sealed thin window "pancake" style G-M detector.

The proportional counter used to measure beta activity is a windowless gas flow counter with a hemispherical sensitive volume and a 2π-steradian collection geometry. This counter has a 0.5-mm thick steel sample support tray. This support acts as a beta backscatter which is approximately infinitely thick for backscattering purposes when beta energies are below 1.0 MeV. Two pure silver backscatterers, also approximately infinitely thick, were used as foil supports during some of the counts.

The G-M counting system used for some of the foil counts was assembled from several components. The GM tube is a Model N1002 made by TGM Detectors. This is a pancake style tube with a halogen fill gas. It has a graphite coated mica window that is 44 mm in diameter and approximately 2.0-mg/cm^2 thick. The anode consists of a thin stainless steel ribbon and its stainless steel case forms the cathode (17:4). At 6.4 mm from the tube window the sensitive volume subtends a solid angle of 4.55 steradians for a point source. Both the detector tube and a movable sample tray are mounted in an enclosure fabricated from 2" x 4" x 8" lead bricks. Additional shielding from background radiation is provided by stacking similar lead bricks around this enclosure. The two silver backscatterers used with the 2π counter were also used with this setup. This detector configuration and shielding arrangement is pictured in Figure 5.

Two radioactive standard sources were used in setting up the proportional and G-M counting systems, and in routine system stability tests. A ^{204}Tl point source was used with the proportional counter. A Ra-DEF (^{210}Pb-^{210}Bi-^{210}Po) source was used with the G-M counter because

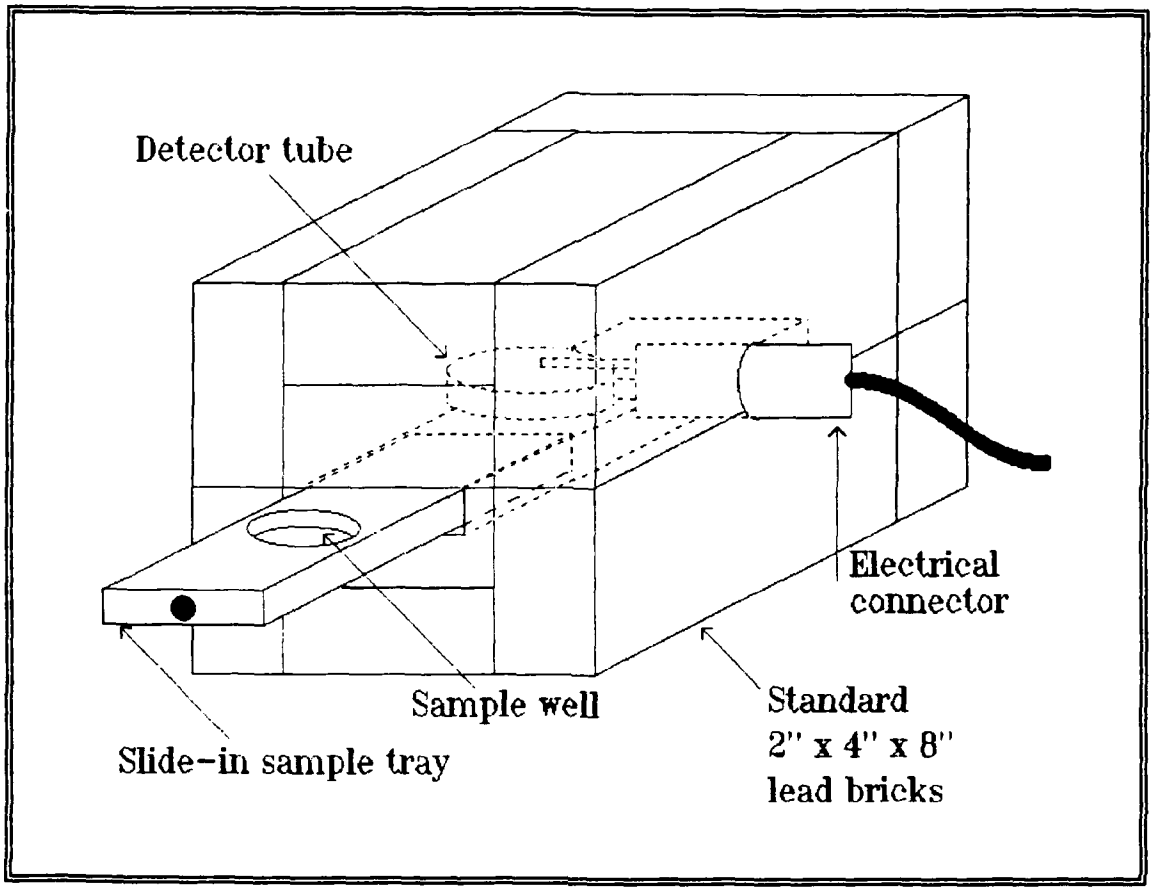

Figure 5. G-M Counter Configuration and Shielding Arrangement

the count rate from the ^{204}Tl is so high it saturates the G-M tube. The Ra-DEF source was covered with 0.05 mm of aluminum foil to absorb all but the 1.16-MeV beta emission. This radiation and the 0.76-MeV beta radiation from thallium are reasonably close in energy to the 0.962-MeV beta decay from ^{198}Au.

Pu-Be Source and Foil Suspension Bar

While calibrating the flux integrators and Bonner spheres it was required that some of the foil irradiations be made under conditions where there was as little neutron scattering as possible. A simple hanger was fabricated to permit raising the neutron source and detectors high above any objects that might scatter neutrons. This device is shown in figure 6.

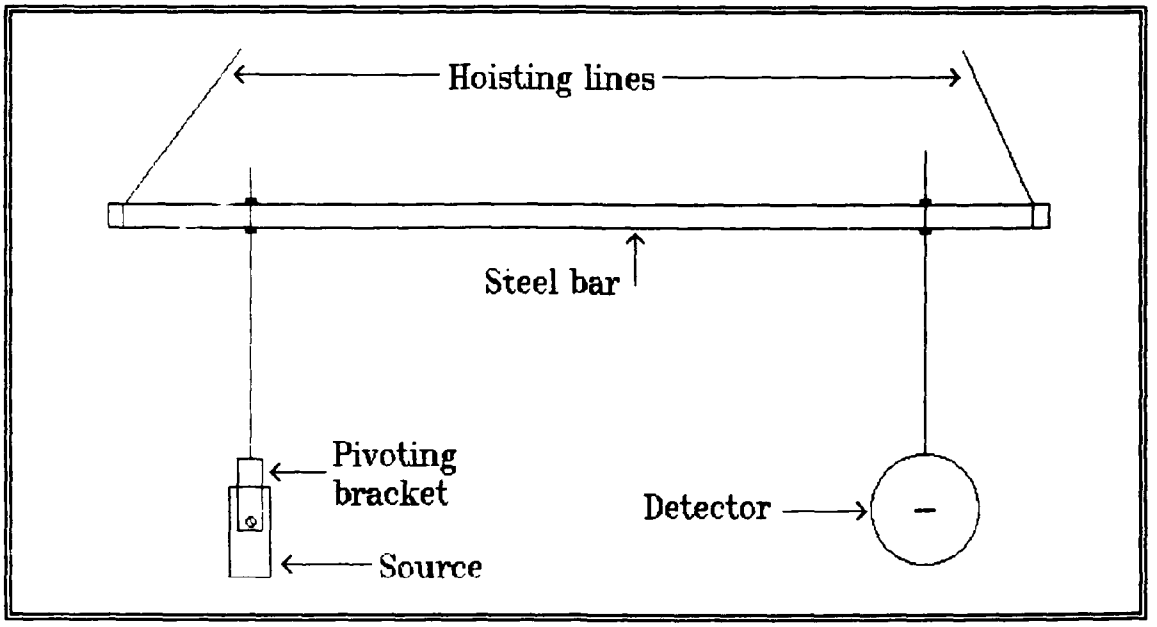

Figure 6. Source-Detector Hanger Configuration

The hanger has a stainless steel pipe as a crossbar, with eight holes drilled 25 cm apart. This permits source-to-detector spacings of 25 cm to 175 cm. Vertical alignment was achieved by using threaded steel rods with jam nuts to hang the source and detector from the crossbar. A simple yoke fixture made out of aluminum sheet both supported the neutron source and allowed it to be rotated about its center. The source bracket was indexed with punch marks in 22.5° increments. The entire assembly was hung from the overhead of the decommissioned reactor dome of WPAFB Building 470. All solid objects inside the dome were six meters or more from the hanger during the irradiations that are later described as "low scatter".

Computer Resources

The NRL codes NEWBUNKI.FOR and TEST10.FOR were compiled from FORTRAN IV source code and run under the VAX/VMS operating system on a DEC VAX/11-780. The program FOIL5.BAS, the source listing for which is contained in Appendix D, was used for all of the foil activity calculations. FOIL5.BAS was written by this author in Microsoft QuickBasic,

Version 4.00b. The code was compiled and run under MS-DOS, Version 3.30+ on a Zenith Z-386 Desktop Computer with an Intel 80387 numeric coprocessor installed.

IV. Experimental Procedure and Results

Several calibrations and verifications were made while devising a neutron detection system for hospital use. Initially the two proportional counter configurations and the G-M counter were calibrated. All of the counting corrections required to determine A_s for gold and indium were calculated or extracted from published information. A set of cross-calibration constants for the three detector configurations was then determined. By using information gained from the counting system calibrations, a calibration constant for the flux integrators was found. This constant relates A_s of a foil irradiated in the flux integrator to the magnitude of the activating flux. Following these experiments, two sets of gold foils were irradiated with the same neutron source used to calibrate the flux integrators. The results from this pair of experiments were used to select a suitable unfolding algorithm for and to assess the accuracy of Bonner sphere spectrometry. A set of irradiations was made in an x-ray therapy facility using three neutron detection methods which included gold foil activations using Cd-difference pairs, flux integrators, and Bonner spheres. In this chapter the experimental procedures that were used are described and results are described and compared. All of the quoted error estimates are in terms of $\pm 3\sigma$ unless otherwise stated. Likewise, the error bars depicted in the graphical results represent a range of uncertainty of $\pm 3\sigma$. For reporting purposes the cadmium-cutoff energy is assumed to be 0.68 eV rather than 0.5 eV. Research within the past twenty years indicates that for the geometries used in this study, the higher cutoff energy better represents the results that are obtained in practice (18:196).

Counting System Calibrations

The beta detector calibrations were made for three counter configurations. Two of these are the same 2π proportional counter. The only

difference is that detector #1 has a thick steel backscatterer and detector #2 has a thick silver backscatter. Detector #3 is the thin window G-M detector with a thick silver backscatterer. All three of these configurations are described in detail in Appendix E. The saturation count rates, C_s from six foil irradiations were used to find μ in the combined counting efficiency factor:

$$f_\gamma(x) f_{bs}(x) f_s(x) = a e^{-\mu x} \tag{12}$$

A pair of foils was irradiated in each of three stringers in the graphite pile. C_s Was calculated for each foil so that equation (14) could be solved for each pair of foils.

$$C_s = b(E) e^{-\mu x} \tag{14}$$

The mean value found for beta mass attenuation coefficient is

$$\mu = (9.86 \pm 1.06) \times 10^{-3} \text{ cm}^2/\text{mg}$$

The data used to calculate μ is listed in Table III.

Table III

Solutions for Equation (14) Using Gold in Detector #1

Stringer Number	Count Number	Foil Thickness [mg/cm^2]	$C_s \pm 3\sigma$ [s^{-1}mg^{-1}]	b(E) [s^{-1}mg^{-1}]	$(\mu \pm 3\sigma) \times 10^2$ [cm^2/mg]
FS1	114	51.9	0.550 ± 0.013	0.932	1.02 ± 0.06
	142	102.4	0.328 ± 0.007		
FS4	104	55.9	0.696 ± 0.009	1.20	1.00 ± 0.05
	150	101.2	0.433 ± 0.009		
FS5	101	50.3	0.350 ± 0.010	0.558	0.935 ± 0.072
	143	102.7	0.213 ± 0.006		

In conjunction with determining μ for detector #1, the first cross-calibration was made between detectors #1 and #2. Clearly, μ for detector #2 must differ from that of detector #1 by an amount equal to the difference in backscatter contributions from steel and silver (4:132). The efficiency factors f_s and f_γ will be unaffected by the change. On the basis of this fact it can be stated that for a single foil counted in both detectors:

$$A_s f_g f_u f_e = C_{s1}/a_1 e^{-\mu_1 x} = C_{s2}/a_2 e^{-\mu_2 x} \qquad (22)$$

In equation (22) the numerical subscripts refer to the beta counter used. A linear regression on nine foils of different thicknesses was used to determine the coefficients in Equation (22):

$$a_1/a_2 = 0.927 \pm 0.028$$

$$\mu_2 = (1.04 \pm 0.11) \times 10^{-2} \text{ cm}^2/\text{mg}$$

A graph of the regression line used to solve for a_1/a_2 and μ_2 is contained in appendix A.

In comparison with detector #2, the cross-calibration for #3, the G-M counter was relatively simple. The main differences between detectors #2 and #3 are the collection geometries and the window absorption for the G-M detector. The ratio a_3/a_2 should, therefore, be equal to f_u for the 2.0-mg/cm^2 thick mylar window of the G-M tube. For such a thin window, an estimate for this factor may be calculated using the equation (19:134):

$$f_u = e^{\mu_u x} \qquad (23)$$

$$\mu_u \approx 0.017/(E_{MAX})^{1.43}$$

where

μ_u is the mass attenuation coefficient of the window for beta particles [cm^2/mg]

E_{MAX} is the endpoint energy of the beta spectrum [MeV].

Using this relation, $f_u = 0.96$. The ratio a_3/a_2 was experimentally measured by counting several foils in both the proportional and G-M counters. The unweighted mean of C_{s3}/C_{s2} for each foil is used as this ratio:

$$a_3/a_2 = 0.941 \pm 0.120$$

In fact, this ratio also compensates for whatever error was made in determining f_g for the G-M detector. The calculated value for f_u is well within the error estimate for a_3/a_2. This empirical constant is used in all subsequent calculations.

To complete the beta detector calibrations, the constant term, a, was calculated using Equation (15). To accomplish this, ten Cd-difference pair irradiations were used to estimate $1/a_2$. From a least-squares fit it was found that $1/a_2 = 1.138 \pm 0.033$. Figure 7 is a graphical representation of the linear regression used to estimate $1/a_2$.

Based on the data reduction from these experiments, the following estimates were made for beta counting efficiency:

Detector #1: $\epsilon = 0.399\exp(-9.86 \times 10^{-3} x)$

Detector #2: $\epsilon = 0.431\exp(-1.04 \times 10^{-2} x)$

Detector #3: $\epsilon = 0.315\exp(-1.04 \times 10^{-2} x)$

In order to judge the reasonableness of the preceding beta counter calibrations, similar counting efficiency factors for indium were used as benchmarks. Clearly, $\epsilon_2[\text{In}] = 0.431\exp(-1.04 \times 10^{-2} x)$ is consistent with $\epsilon_2[\text{In}] = 0.468\exp(-9.69 \times 10^{-3} x)$ (6:58).

In addition to finding counting efficiencies, background count rates (r_{bg}) were measured for the three beta detector configurations. This was done periodically over a six month period with counting times as long as 80,000 sec. Results showed that with either backscatterer in

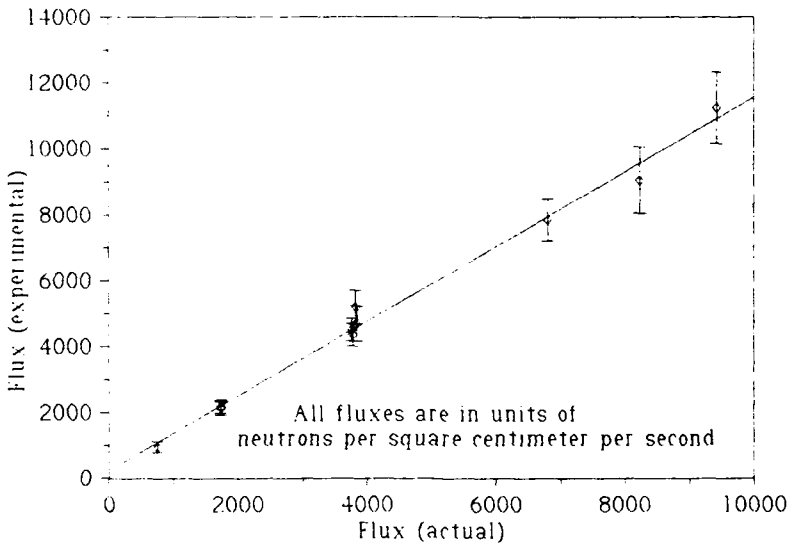

Figure 7. Solution for Equation (6) Using a Linear Regression to Find 1/a for Detector #2.

the proportional counter, $r_{bg} = 0.585$ counts/s . For the G-M counter $r_{bg} = 0.281$ counts/s . The error estimate for both these rates is $\sigma < 0.01\%$.

Flux Integrator Calibration

By using the beta counting corrections described under counting system calibrations, the flux integrators were calibrated as neutron flux meters. The source strength calculations in Appendix B and anisotropy correction from Appendix C were used to calculate the flux from Pu-Be source M1170 at distances of 25 cm to 150 cm in 25-cm increments. Gold foils were irradiated at each of these distances. The saturation activities of these foils are the data from which a calibration constant for the flux integrators was determined.

Ten foils were used for the calibration of the flux integrators. All were approximately 25.4 mm in diameter and 0.025-mm thick. Five foils were irradiated at a source-to-foil distance of 50 cm and one was

irradiated at each of the other distances for which a flux had been calculated. All of the activations were conducted with the foils at 90° with respect to long axis of the source. The saturation activity was then determined for each of the foils. A linear regression of A_s on flux was done so that the inverse of the slope of the regression line could be used as K(E), the calibration constant. The result is that the regression line has the equation:

$$A_s = (3.36 \times 10^{-4})\phi - (1.7 \times 10^{-3})$$

The uncertainty in the slope is $\sigma = 7.0 \times 10^{-6}$ cm²/ $^{1}_{0}$n-mg and the uncertainty in the intercept is $\sigma = 4.5 \times 10^{-3}$ s^{-1}-mg^{-1} . This calibration curve was derived from only eight of the ten data points because the two activities which were more than three standard deviations in A_s from the initial regression line were discarded. The effect of culling these data points was not, however, significant. The slope changed by less than one percent as a result. The final result is that:

$$K(E) = (2970 \pm 180) \ ^{1}_{0}\text{n-mg/cm}^2$$

Where $E = 4.2$ MeV .

In order to validate the calibration constant, three matters were considered. First, it is clear that if flux is inversely proportional to the square of distance from the source, then A_s should exhibit the same proportionality. To check for this, A_s was fit to a power function of d, the source-to-detector distance. Indeed, there is an inverse relationship to d within the limits of uncertainty of the fit. The fit for the data is $A_s = 5.72d^{-1.98}$ with an uncertainty in the exponent of $\sigma = 0.04$. The second consistency check is to verify that the intercept of the fit of A_s to ϕ is zero. A contrary result would indicate that unresolved systematic errors exist in the data. In fact the intercept of the regression line is -1.7×10^{-3} with an uncertainty

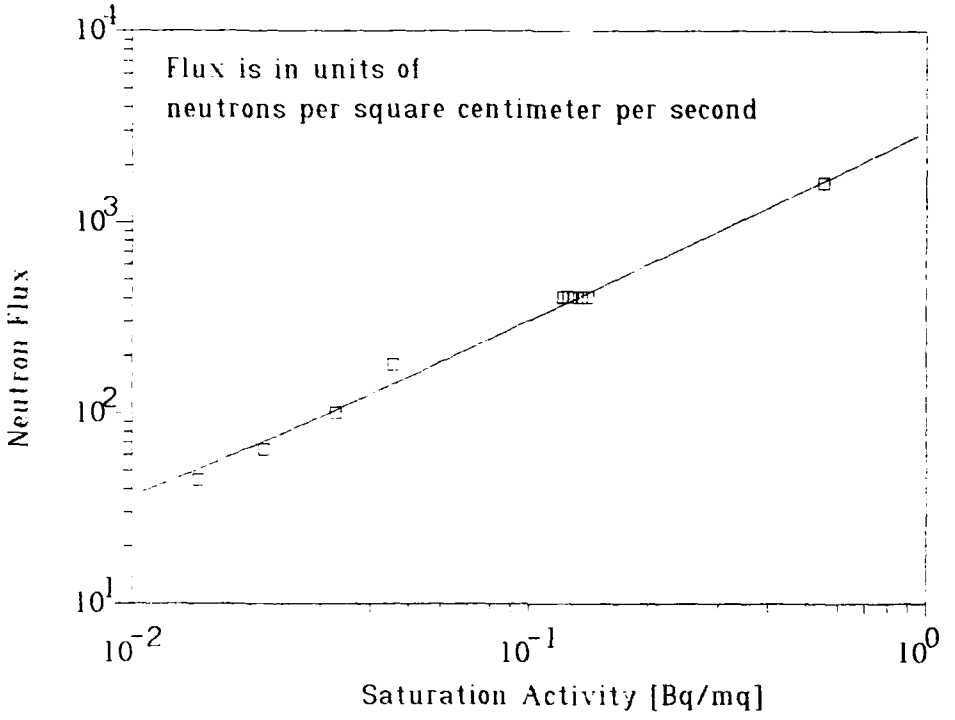

Figure 8. Least-Squares Fit to Find K(E) For the Flux Integrators

of $\sigma = 4.5$. Within the limits of this uncertainty, the intercept is zero. Finally, the uncertainty of the calibration constant ought to be less than that of the individual data points used to calculate it. For K(E), $\sigma_{K(E)} = 60$ $\frac{1}{0}$n-mg/cm^2, which is approximately 2%. In comparison, the uncertainty in the individual data points is $\sigma_{A_s} \approx 4\%$. For eight data points this is excellent agreement. All three of these comparisons support the assertion that K(E) is valid. The linear regression that was used to determine K(E) is depicted in figure 8.

In addition to the system calibration, two other sets of flux integrator irradiations were made in a controlled environment. For one data set, nine foils were irradiated with source M1170 under conditions where there were many scattered neutrons. The other data set was obtained by sending three foils and a flux integrator to SLAC for irradiation with their neutron source. The foils sent to SLAC were returned to AFIT,

where they were counted and A_s calculated for each. All foils for these two experiments were the same 25.4-mm diameter, 0.025-mm thick gold used during the original calibration of the flux integrators.

The saturation activities of the nine foils irradiated at AFIT and the three from SLAC were used for measurements where many scattered neutrons contributed to the total flux. This was done as an approximate check on the accuracy of the flux integrators for other than the very narrow energy distribution of the Pu-Be source spectrum. The measurements made at AFIT were with source-to-foil distances of 25 cm to 125 cm in increments of 25 cm. Source M1170 and all foils were suspended 25 cm above a homogeneous concrete plane. The foils were irradiated in one of the four identical flux integrators. The irradiations at SLAC were also made in one of these four. The SLAC foils were activated at distances of 25 cm, 50 cm, and 100 cm from their source. These activations were made at source and foil heights of two meters above a uniform concrete plane. All of the foils were counted at AFIT using the methods described elsewhere in this section.

The saturation activities for the foils irradiated under high-scatter conditions were multiplied by K(E) to arrive at a measured neutron flux. A calculated flux was found for each of these foils using known source strength plus a scatter contribution calculated in appendix F using Jenkins' method. The uncertainty in the ratio of the total to direct fluence is $3\sigma \approx 5\%$ with this method (20:45). Figure 9 is a representation of the results from the high-scatter irradiations. The foils irradiated at AFIT are plotted along with those irradiated at SLAC. The vertical error bars indicate a 3σ range of uncertainty in the measured flux. The horizontal error bars indicate the 5% range of uncertainty in calculated flux. Ideally, calculated and measured flux will be equal. This is what the solid line in Figure 9 represents. Figure 10 presents the same data as in Figure 9, but for clarity, only shows a range of fluxes up to 600 $\frac{1}{6}n/cm^2$-s.

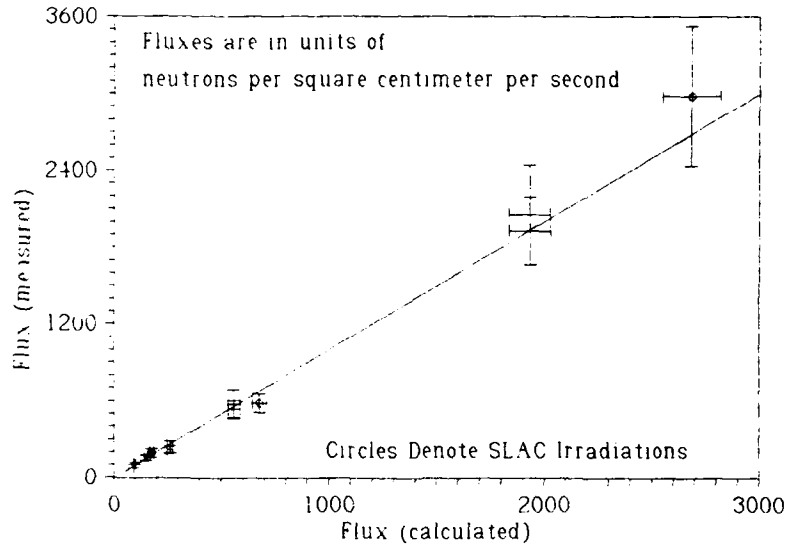

Figure 9. Measured Flux vs. Calculated Flux For the Flux Integrators When Used Under High-Scatter Conditions

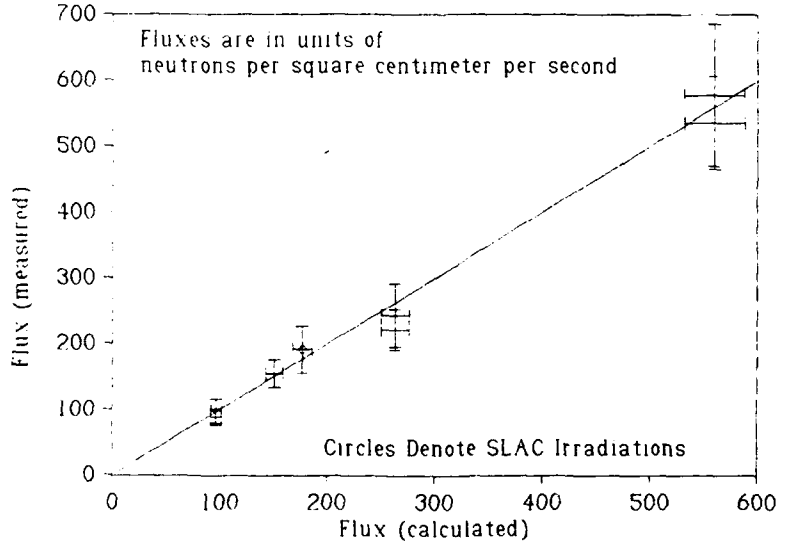

Figure 10. Magnified View of Figure 9

It is clear from these high-scatter irradiations that the flux integrator is a good, but not perfect neutron flux meter. Two of twelve data points are more than 3σ from the expected result, one of which comes from a SLAC irradiation. It is unlikely that the scattered flux calculation is responsible for these deviations because there is no obvious trend toward larger deviations as the scatter contribution increases. Likewise, it is doubtful that an inaccuracy in the thickness-dependent counting corrections would explain the errors. One of the foils was substantially thinner than the norm for this set, and the other was much thicker, yet both had activities which resulted in a measured flux that was too low. Finally, both of the stray data points come from foils counted with detector configuration #1, for which the most direct calculation of counting corrections was made. For these reasons it must be concluded that random procedural errors caused the anomalous results. The rest of the data is well correlated to the function $\phi(\text{measured}) = \phi(\text{calculated})$ with a correlation coefficient of $r = 0.995$. Thus, the flux integrators are acceptably accurate when used with the empirically determined calibration constant.

Bonner Sphere Set Calibration

The Bonner sphere set previously described was tested with Pu-Be source M1170 to investigate its response. Two sets of seven foils each were activated using one bare foil and a foil in each of the six spheres for each set. All foils were pure gold with approximate dimensions of 12.7-mm diameter and 0.051-mm thickness. One set of foils was activated under conditions of negligible neutron scattering, while the second was done under high-scatter conditions.

The high-scatter activations were conducted with a source-to-foil separation of 100 cm. All foils were irradiated simultaneously, one in each of the six spheres and one bare. The source was suspended using the hanger at 25 cm above a concrete plane, while the spheres were placed on small plywood stands to put the foils 15 cm above the concrete

plane. The seven detectors were equally spaced on the circumference of a circle with a 100-cm radius. As a matter of convenience in arranging the experiment the source was not placed at the same height above the ground plane as the spheres. The accuracy of the ground scatter calculation is not impaired by using different heights for the source and detector.

Table IV

Gold Foil Saturation Count Rates for Bonner Sphere Irradiations with Pu-Be Source M1170

Count Number	Scatter Conditions	Bonner Sphere	A_s [s^{-1}]	σ_{A_s} [s^{-1}]
51	LOW	BARE	0.25	0.24
47	LOW	2"	0.79	0.24
45	LOW	3"	1.91	0.21
46	LOW	5"	5.38	0.59
48	LOW	8"	8.35	0.82
49	LOW	12"	4.78	0.53
50	LOW	12"	4.78	0.53
66	HIGH	BARE	0.40	0.07
67	HIGH	2"	0.89	0.11
68	HIGH	3"	2.49	0.30
69	HIGH	5"	4.97	0.49
70	HIGH	8"	6.09	0.73
71	HIGH	10"	5.03	0.60
72	HIGH	12"	3.33	0.33

The low-scatter activations were made using the same set of Bonner spheres as for high-scatter conditions, with a similar set of foils. The activations were done singly for three of the foils and in pairs for the other four because the hanger could only support one or two spheres at a time. The source-to-foil distance was 75 cm for each detector in this set. All of these irradiations were made at least 6 meters from any solid object. Table IV gives a summary of foil counting results for

both sets of irradiations.

The values of σA_s presented in table IV vary between 9.0% and 11.2%. This large uncertainty results from the fact that the foils irradiated in Bonner spheres were relatively thick ($x \approx 100$ mg/cm^2). For foils of increasing thickness the uncertainty in μ becomes the dominant factor in the uncertainty in A_s because of the exponentiation in the relation $f_v f_{bs} f_s = ae^{-\mu x}$. Since all of these foils had thicknesses within a few percent of each other the loss of accuracy is not accompanied by a loss of precision. The significance of this fact is that even though the total neutron flux calculated from these A_s values may be inaccurate, the shape of the neutron spectrum will be unaffected by this kind of calibration error.

The three spectrum unfolding algorithms were tested using the foil data from two Bonner sphere irradiation sets. The results of these tests were used to select the "best" unfolding algorithm and initial spectrum. This selection is highly subjective because the decision is made on the basis of which routine produces the most reasonable unfolded spectrum. It is this "reasonableness" criterion which leaves the choice open for argument. Many researchers have investigated the response of a Bonner sphere set as a neutron spectrometer. Based on Johnson's work (10) an initial decision was made to limit testing to only a few initial spectra. In all cases Sanna's response matrix was used (21).

The unfolding algorithms tested were BON31G, YOGI, and SPUNIT. BON31G is the oldest of the iterative recursion routines in use today (10:2). YOGI is a more recent code developed at NRL (9:6). SPUNIT is an algorithm similar to BON31G that was coded at Pacific Northwest Laboratories based on the work of Dorashenko (10:2). For each of these routines three assumed spectra were used as inputs. One of these was a straight 1/E spectrum, while the second was a step function where the 1/E input was split at 450.8 keV. Each of the two steps were 1/E dependent, but the high-energy bins were given an initial magnitude ten

times that of the lower energies. The third initial spectrum was the so-called "MAXIET". This is a superposition of fast and thermal energy Maxwell-Boltzmann distributions with a 1/E distribution at intermediate energies. In order to limit the number of test cases, all of the calculations were made without smoothing or shape modifications. For the MAXIET inputs an initial value of (3/2)KT = 4.2 MeV was used for the high-energy Maxwellian.

The first Bonner sphere test was made with neutron source M1170 under conditions of negligible scatter. The calculated spectra from all three algorithms are presented in figures 11, 12 and 13. Here, as in all subsequent cases, the data points represent the integral flux for each energy bin in units of $^{1}_{0}n/cm^{2}$-s.

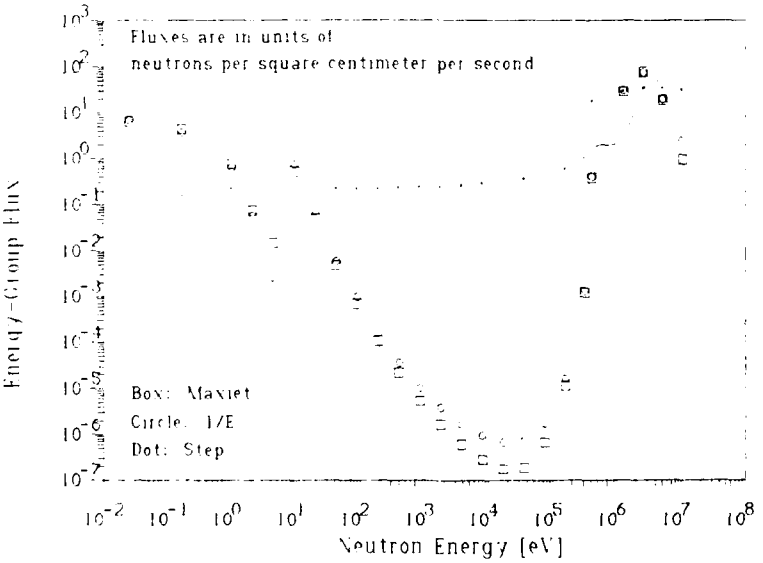

Figure 11. BON31G Results For a Pu-Be Neutron Source Using Three Initial Spectra

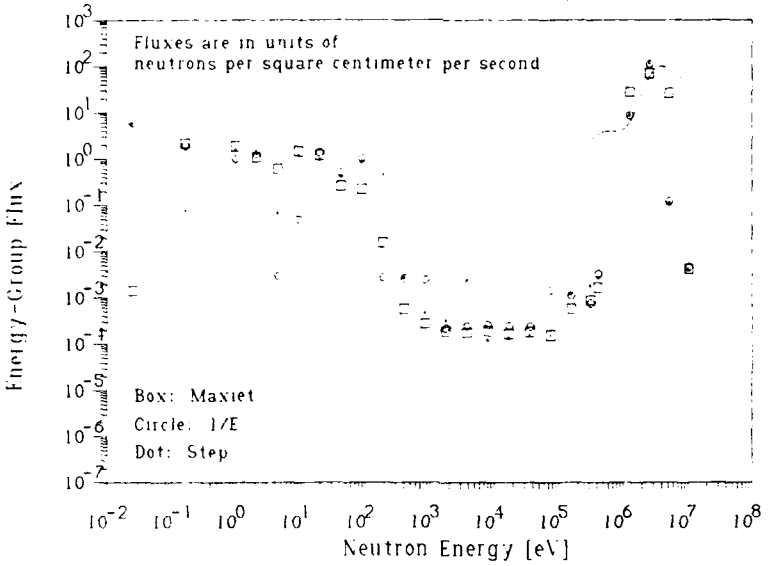

Figure 12. YOGI Results For a Pu-Be Neutron Source Using Three Initial Spectra

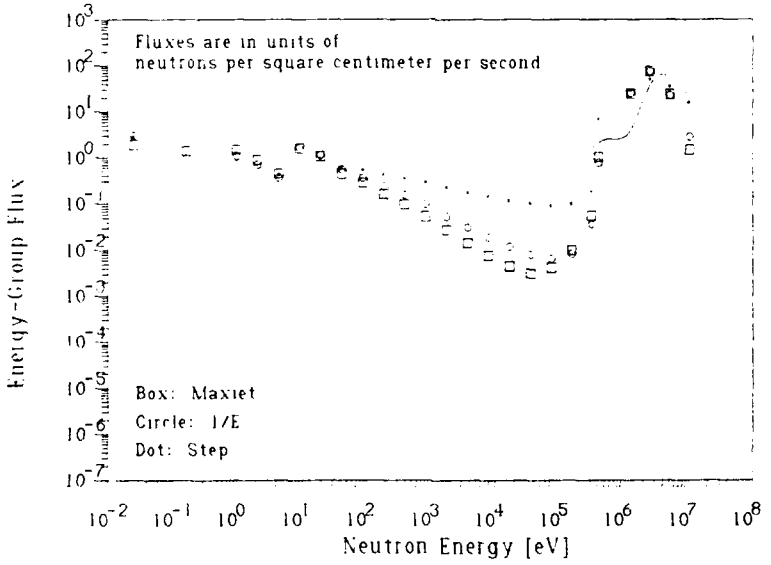

Figure 13. SPUNIT Results For a Pu-Be Neutron Source Using Three Initial Spectra

The fluxes from all of the Bonner sphere results are plotted at the log-mean energy for each bin. The known spectrum of a Pu-Be source, from figure 1, was re-binned to the energy groups used by the unfolding algorithms and overlaid on the experimental results as a solid line.

TABLE V

Flux and Dose Results from Bonner Sphere

Tests with a Pu-Be source Under Low-Scatter Conditions

Unfolding Algorithm	Input Spectrum	Average Neutron Energy [MeV]	Flux [$\frac{1}{6}$n/cm^2-s]	Dose [rem/s]
BON31G	MAXIET	2.62	140	5.00 X 10^{-6}
BON31G	1/E	2.71	141	5.01 X 10^{-6}
BON31G	STEP	4.20	152	5.44 X 10^{-6}
SPUNIT	MAXIET	2.73	136	4.93 X 10^{-6}
SPUNIT	1/E	2.80	137	4.95 X 10^{-6}
SPUNIT	STEP	3.57	144	5.42 X 10^{-6}
YOGI	MAXIET	2.67	135	4.94 X 10^{-6}
YOGI	1/E	2.36	137	4.91 X 10^{-6}
YOGI	STEP	2.37	136	4.91 X 10^{-6}

A comparison of Figures 11 through 13 reveals some interesting results. First, all of the codes produced essentially the same total flux and dose estimates under all conditions, as summarized in Table V. Most notably, the SPUNIT results appear to be least influenced by the choice of initial spectrum. It is also the only algorithm which appears to resolve the plateau in the several-hundred-keV energy range. The breadth of the high-energy peak from SPUNIT is also most realistic. The 1/E and MAXIET results in figure 13 were taken from 1000 iterations of the code, but even after only 300 iterations the spectrum had essentially converged to a final set of results. A 5% error criterion was met in these 300 iterations. In contrast, BON31G was never able to meet a 5% error criterion, even after 1000 iterations. The YOGI results are somewhere in-between BON31G and SPUNIT. YOGI is rapidly convergent,

meeting the 5% criterion in less than 360 iterations in every case. YOGI does, however, oscillate markedly for this case.

In isolation, the low-scatter results are not conclusive. The Pu-Be source spectrum loses all of its distinctive peaks when re-binned to the fairly broad energy groups of the Bonner sphere set. There is nothing remarkable from which to draw any conclusions about the reasonableness of the results. Consequently, the high-scatter irradiation set was made to provide some additional information for qualitative comparison. YOGI was used for the spectral deconvolution to see whether a neutron spectrum with a broader energy distribution changed the general behavior of this unfolding algorithm. Figure 14 is the graphical result from this irradiation set.

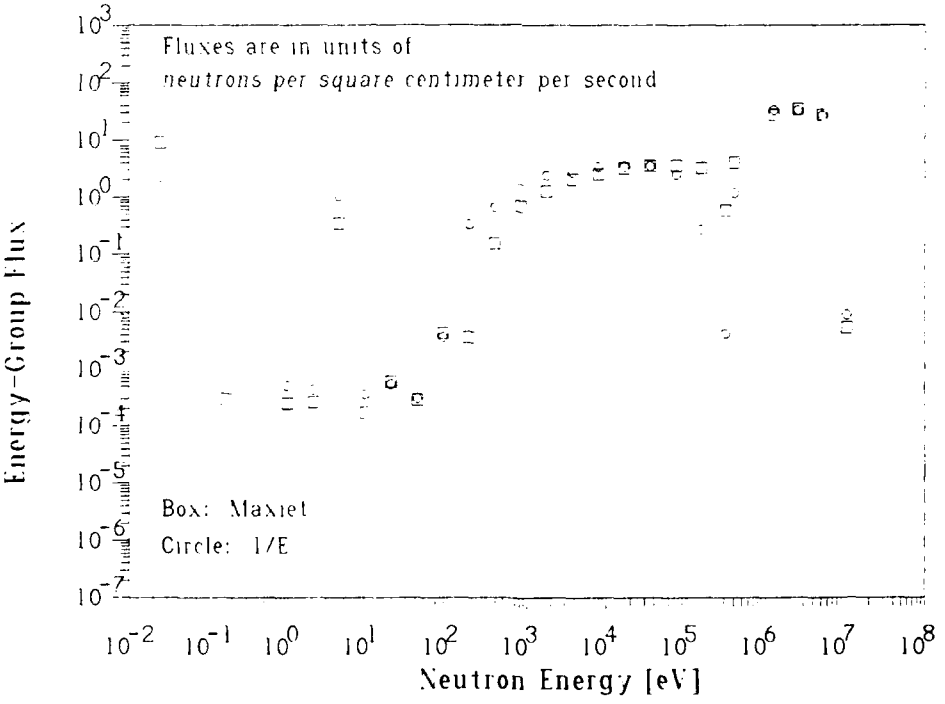

Figure 14. YOGI Results For a Pu-Be Neutron Source Under High-Scatter Conditions

In the high-scatter case YOGI seems to perform better than in the low-scatter experiment. The oscillations are less marked and the results appear to be less dependent on the input spectrum. For this data set the algorithm converges very rapidly. Both calculated spectra in figure 14 meet an error criterion of less than 1.4%. This was achieved in 240 iterations for the MAXIET input and 447 iterations for the 1/E initial spectrum. The calculated flux is 126 $\frac{1}{0}n/cm^2$-s using the MAXIET input and 120 $\frac{1}{0}n/cm^2$-s using the 1/E input.

All three of the unfolding algorithms appear to have their own particular strengths and shortcomings. It is not surprising that the MAXIET input gives more rapid convergence in every case. The physics of photoneutron production predicts that the spectrum will be of this form. For this reason MAXIET is used as the input spectrum for the Miami Valley Hospital experiments. It might also be concluded that the SPUNIT algorithm is superior to the other two. In fact, the limited testing of all three codes is insufficient to support that assertion. The SPUNIT algorithm is similar to BON31G in that it systematically perturbs the input spectrum bin by bin, from low to high energies. It does this using a fixed perturbation on every iteration. For this reason it will tend to be less oscillatory than YOGI, even without smoothing, because the algorithm inherently tends to smooth the result. YOGI uses a random perturbation, starting at a randomly selected energy bin. Since the object of this study is to measure an unknown neutron spectrum, the least biased algorithm is the most desirable. On this basis YOGI is inherently superior to the other two codes, therefore only YOGI was used in the hospital irradiations.

Miami Valley Hospital Experiments

The culmination of all the experimental investigations conducted was the employment of the various detectors in a real x-ray therapy environment. Several irradiations were made at Miami Valley Hospital using their 45-MeV Betatron in the x-ray mode. All three types of gold

foil irradiations were made. The foil positions for these irradiations are reported in terms of a cylindrical coordinate system whose origin is at the center of the betatron's platinum bremsstrahlung target. The z coordinate is reported in centimeters below target center, the r coordinate is the radial position in centimeters from the beam axis, and the θ coordinate is reported in degrees from an arbitrary reference line along the long axis of the horizontal treatment table and aligned in a direction directly away from the wall upon which the machinery was mounted. Figure 3 in the experimental equipment section gives a schematic representation of the treatment room layout.

Thermal neutron flux was determined absolutely by the cadmium-difference method at four locations using 25.4-mm diameter, 0.025-mm thick gold foils. Covers for the Cd-clad foils were 0.75-mm thick. For each pair, both foils were irradiated simultaneously at center-to-center distances of approximately 5 cm. These pairs were irradiated at distances of 20 cm, 30 cm, 50 cm, and 100 cm from the x-ray beam axis. Activations at 20 cm and 30 cm were conducted simultaneously without any other detectors present. Activations at 50 cm and 100 cm were conducted concurrently with the subsequently described Bonner sphere activations.

Five 25.4-mm diameter, 0.025-mm thick foils were activated using the 6" cylindrical detectors, to measure total epicadmium flux in the vicinity of the treatment table during x-ray therapy. One measurement was made 100 cm from the beam axis with no other detectors present. Two measurements were then made simultaneously at distances of 20 cm and 30 cm from the beam axis, with a center-to-center spacing between detectors of 50 cm. Two more measurements were made concurrently with the Bonner sphere irradiations at distances of 50 cm and 100 cm from the beam axis.

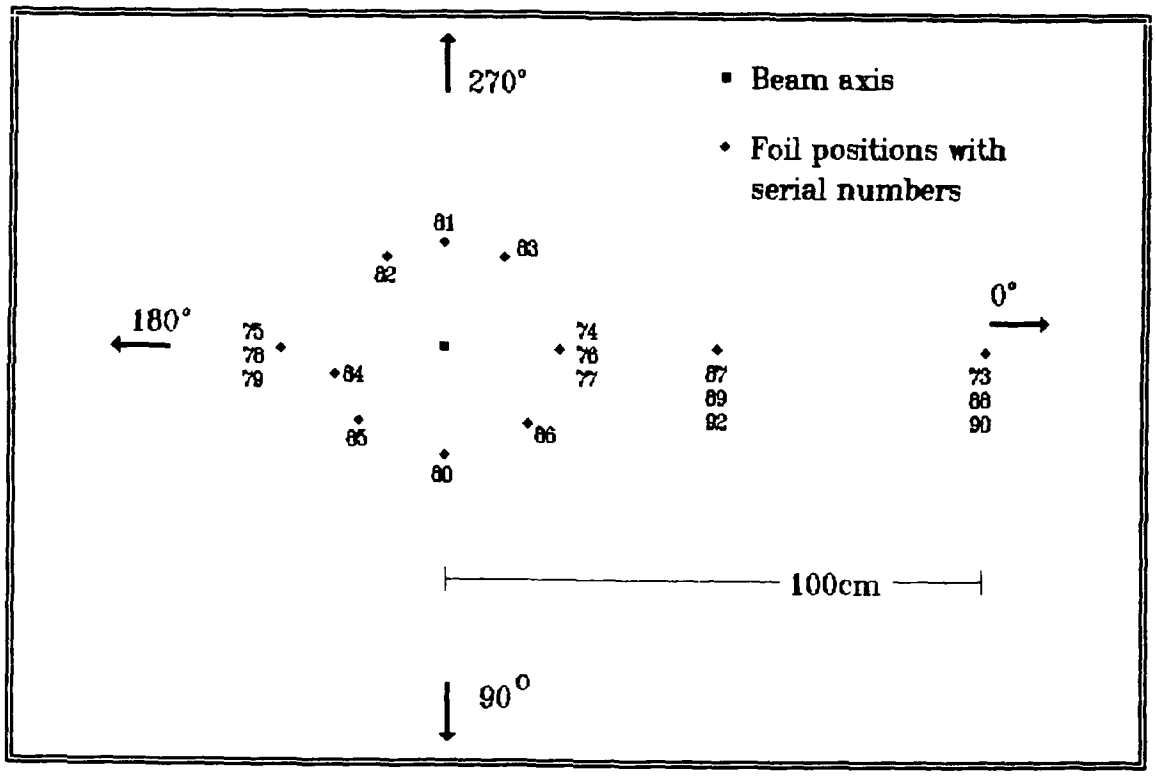

Figure 15. Foil Locations for MVH Tests

The foils in the Bonner spheres and the associated bare foil were irradiated simultaneously. These foils were 12.8 mm in diameter and 0.050-mm thick. A diagram of the positions of the thirteen foils irradiated together is depicted in figure 15.

All foils activated at Miami Valley Hospital were subsequently counted in either of the two beta counting systems previously described. All of the appropriate counting corrections were applied to the raw data to obtain a saturation activity in Bq/mg. An important departure from the method employed in the laboratory was dictated by the operating characteristics of the betatron. This unit could not be run continuously for more than five minutes due to system cooling limitations. Consequently, all except one of the foils were irradiated for six periods of five minutes each, with approximately two minutes waiting time between periods. Because of the relatively long half-life of the gold

activation product this will not introduce a significant error over assuming a continuous thirty minute exposure ending at the same time that the last actual irradiation ceased. An upper bound may be placed on this error by comparing two limiting cases. The first case is where there are no breaks in irradiation and irradiation ceases at time t_e. The opposite extreme is when irradiation ceases at a time $t_e - t_d$; where t_d is the sum of the delays interspersed with the irradiations. The ratio of activities of the two foils will then be:

$$A_2/A_1 = e^{-\lambda t_d}$$

For these tests $\lambda = 0.0107/hr$ and $t_d = 0.267$ hr with a ratio of $A_2/A_1 = 0.9972$. This error may be disregarded because the magnitudes of the counting errors involved are at least ten times larger.

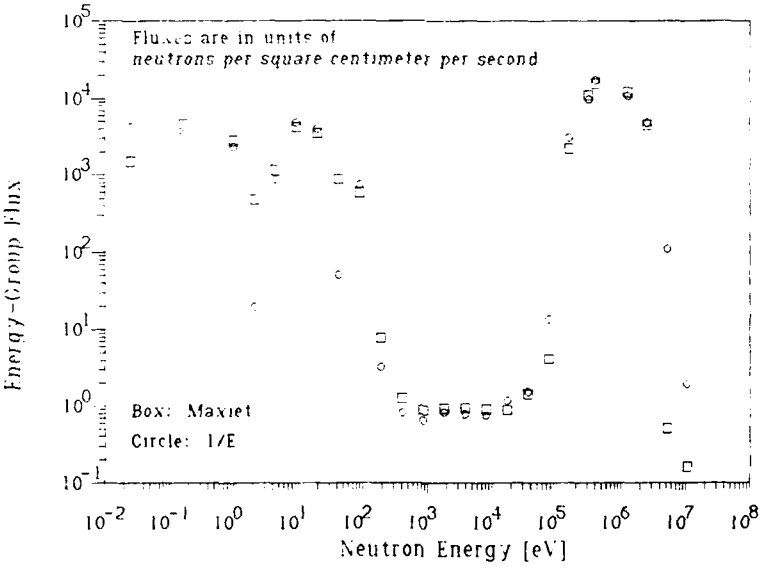

Figure 16. Neutron Spectrum Deconvolution Using YOGI for Irradiations at Miami Valley Hospital

Figure 16 depicts the Bonner sphere results from the hospital experiments. Both MAXIET and 1/E input spectra were used, with similar

results. In both cases the average difference between calculated and actual count rates (the error criterion) was approximately 3.3%. This result was attained after 158 iterations with the MAXIET input and 186 iterations with the 1/E initial spectrum. YOGI still exhibits some oscillation in this example, but with the MAXIET input this effect is minimal. It was previously stated that the anticipated spectrum has a 1/E dependence at intermediate energies. That assertion is only an approximation because it is based on the assumption that the neutrons undergo multiple scatters in a moderator with little absorption. The treatment room is not a particularly good moderator, nor is it likely that it exhibits low levels of neutron absorption. As a result, the actual spectrum should exhibit an intermediate energy distribution which is "flatter" than 1/E. YOGI's relatively flat spectrum in the energy range of 300 to 30,000 eV is, therefore, a reasonable result.

Comparison of Results From the Three Neutron Detection Methods

Since more than one neutron detection method was used to measure each of the sources, it is worthwhile to compare the results directly. Table VI lists the epithermal flux measurements obtained from the flux integrator and the Bonner spheres. The low-scatter result for the flux integrator is not included because this measurement is one which was considered anomalous during the original calibration tests.

Table VI

Neutron Flux Measurements with Pu-Be Source M1170

Scatter Conditions	Detector	$\phi_{epithermal}$ [$^{1}_{0}$n/cm^2-s]	
		(measured)	(calculated)
Low	Bonner spheres	133	179
	Flux Integrator	155	151
High	Bonner spheres	117	151

Only the Bonner sphere results using YOGI with a MAXIET input are reported because this is the unfolding algorithm of choice. In fact, all of the unfolding codes produced similar results, as it was noted previously. Interestingly, the Bonner spheres produce an epithermal flux measurement which averages 24% lower than calculations predict. Sanna has indicated that his response matrix has never been formally tested (22). The present results indicate that there may be a need to introduce a calibration factor into the unfolding algorithm when this response matrix is used for absolute measurements of flux and dose.

Table VII

Neutron Flux and Dose Measurements From a 45-MeV Betatron

r [cm]	z [cm]	Detector	ϕ(thermal) [$\frac{1}{0}$n/cm^2-s]	ϕ(epithermal) [$\frac{1}{0}$n/cm^2-s]
		Flux Integrator	---	48,400
		Cd-Difference Pair	4,060	---
20	125	Bonner Spheres	6,210	59,300
		Flux Integrator	---	60,900
30	125	Cd-Difference Pair	3,190	---
	125	Flux Integrator	---	40,000
50	133	Cd-Difference Pair	4,560	---
	125	Flux Integrator	---	23,300
100	133	Cd-Difference Pair	2,270	---

All three neutron detection methods were used at Miami Valley Hospital. The results from these measurement are consolidated in Table VII. The "r" and "z" columns refer to foil positions with respect to the center of the betatron's platinum target, as described under Experimental Apparatus.

When the betatron is used as the neutron source, the Bonner spheres give a larger flux than the flux integrators. This is just the opposite of the results from the Pu-Be source irradiations. The discrepancy may be the consequence of a greater energy dependence than anticipated for

the flux integrators, even though the experiences of others tend to dispute this possibility. A more likely explanation is that the close spacing of the spheres caused an abnormal amount of neutron scattering, thereby inflating the magnitude of the measured flux. The methodology of Bonner sphere spectrometry must be improved in this respect. As a representative test it is still a useful result that YOGI can establish a proportionality between fluence and dose. It was found that for this particular spectrum:

$$\text{Dose Rate Equivalent} = 1.18 \text{ mrem/s}$$

$$\phi(\text{total}) = 65{,}000 \ {}^{\text{1}}_{\text{0}}\text{n/cm}^2\text{-s}$$

therefore

$$H = (1.80 \times 10^{-5} \text{ mrem-cm}^2 / {}^{\text{1}}_{\text{0}}\text{n})\Phi$$

where

H is neutron dose equivalent [mrem]

Φ is fluence [${}^{\text{1}}_{\text{0}}\text{n/cm}^2$]

At $z = 125$ cm , the photon dose rate is 0.774 rad/s, therefore this particular machine induces a neutron dose rate equivalent of 1.52 mrem/(photon Rad). In comparison, table 15 of NCRP 79 contains the results from several measurements of neutron dose from the BBC Asklepitron 45. When each is converted to units of mrem/(photon Rad) using the conversion factors presented in this section, it is found that the dose rates vary from 0.064 to 3.28 mrem/(photon Rad). Almond reports a measurement of 2.1 mrem/(photon Rad) for this same machine (23:134). The variation in reported measurements is not unreasonable because the neutron output from these machines is strongly dependent on the alignment and adjustment of the beam collimators.

V. Conclusions and Recommendations

The results presented in this study answer some, but not all of the questions posed at the outset of the research effort. The overall intent has been to describe and test a system of neutron dosimetry that is usable in a cancer therapy environment. To this end the original objective has been met. The theory of the three detection methods is coherent and the method conceptually complete. It has been demonstrated that the execution of these methods is straightforward. The monitoring of patient neutron exposure using flux integrators and cadmium-difference pairs is straightforward enough that medical technicians could routinely perform these tasks with a minimum of training. Bonner sphere spectrometry is more involved, therefore requiring more skilled laboratory workers for its execution. It has also been noted that the accuracy of the various calibration factors and corrections is not as good as it could be. An improvement in these results is necessary before the methods can be wholehearted endorsed.

The first set of recommendations is intended to address questions concerning the reliability of the flux integrators. Laboratory experiments with a Pu-Be source show that this detector is a repeatable, reasonably accurate flux meter. Field testing of this method was, however, inconclusive because the betatron neutron source strength is unknown. A useful supplement to the flux integrator calibration would be to repeat the appropriate procedures with an americium-lithium source of known strength. This would verify the energy independence of the detector and provide a calibration constant at neutron energies closer to those of an electron accelerator. The use of borated rubber instead of cadmium as a sheath for the cylinder would also be worth experimenting with. Boron is not as "sharp-cutting" a thermal neutron filter as cadmium, but it has the desirable property of having a very low cross-section for photoneutron production. The use of borated rubber would therefore allow

placement of the detector near or in the x-ray beam without much likelihood of detecting spurious photoneutrons produced in the cylinder sheathing.

Unlike the flux integrators, the reliability of cadmium-difference pairs is completely dependent on the accuracy of the counting corrections that are used to calculate foil activity. The method that was used to determine ϵ is conceptually correct, but could be refined in its execution. Rather than make an assumption about the dependence of ϵ on foil thickness it would be better to activate foils of many thicknesses in a constant flux. This is what Greenfield et al. did. In this way the indirect method that was used could be avoided. There is no reason why the uncertainty in ϵ could not be reduced to a value of approximately 2%, instead of the 10% standard deviation estimated in this study.

Finally, the reliability of the Bonner spheres and especially Sanna's response matrix for gold must be verified. Bonner sphere results are only as accurate as the foil activities that they depend on. Thus, the same counting corrections that affect the cadmium-difference pair results will affect the Bonner spheres. Also, the choice of unfolding algorithm and initial spectrum was very subjective. It would be prudent to evaluate this detector's response more quantitatively. To do so requires a neutron source with a spectrum similar to the x-ray machine that is to be monitored. The objective is, of course, to select the best unfolding algorithm. Without a known source having a broad energy distribution there is really no objective basis for choosing one code over another. Such testing may be beyond the capability of AFIT laboratory facilities because of source availability. Cooperation should be sought from an outside agency possessing sources with the requisite characteristics.

The basic motive for conducting this research was to provide a recommendation for neutron monitoring to Wright-Patterson AFB Medical Center. A proposed procedure is contained in Appendix G. In order to support these recommendations, a computer program which simplifies flux and dose calculations is being provided separately. The code uses flux integrator and cadmium-difference pair irradiations to determine neutron dose-equivalent in rem. The source code is also provided so that when more accurate foil counting corrections are determined they may be easily incorporated. Finally, it must be understood that these recommendations are conditional because they prescribe the use of a Bonner sphere set which is probably not accurately calibrated.

Appendix A: Foil Counting Corrections

The determination of neutron flux by any of the foil activation methods depends on being able to calculate foil saturation activity from beta counts. This is because in a constant flux, saturation activity is equal to the reaction rate of neutrons with the nuclei of the foil material. What follows is a development of equation (7), the relationship between saturation activity and recorded counts.

When a material such as ^{197}Au is exposed to neutrons in a constant flux, the activation product, ^{198}Au, will decay according to the following relation:

$$\frac{dN}{dt} = R - \lambda N \tag{A1}$$

where

N is the number of product nuclei extant at any time

R is the formation rate of the product nuclide

λ is the product nuclide decay constant.

The solution for the differential equation in (A1) can be easily shown to be:

$$\lambda N(t) = R(1 - e^{-\lambda t}) \tag{A2}$$

If the initial activity of the foil material is zero, $\lambda N(t)$, the induced foil activity, will be equal to the total activity, $A(t)$. If the foil were irradiated for an infinitely long time equation (A2) shows that the activity would equal the reaction rate. $A(\infty)$ is referred to as A_s, the saturation activity. It is clear now that:

$$A_s = A(t_e)/(1 - e^{-\lambda t_e}) \tag{A3}$$

where

t_e is the length of the irradiation.

If the foil activity is not counted immediately upon completion of irradiation a correction must be applied to account for the decay in activity during this "waiting time." The loss in activity will be described by the relation:

$$A(t_e + t_u) = A(t_e)e^{-\lambda t_u}$$

where

t_u is the elapsed time from the end of irradiation to the start of counting.

Therefore:

$$A(t_e + t_u) = A_s e^{-\lambda t_u}/(1 - e^{-\lambda t_e}) \qquad (A4)$$

The decaying activity of the foil at time $t_e + t_u$ may be used to calculate the number of disintegrations which take place during a counting time of t_c by performing the following integration:

$$\textit{total disintegrations} = \int_0^{t_c} A(t_e + t_u)e^{-\lambda t}\,dt$$

$$= \frac{A(t_e + t_u)}{\lambda}(1 - e^{-\lambda t_c}) \qquad (A5)$$

It should be recognized immediately that "*total disintegrations*" is simply C_{net}/ϵ, therefore $A(t_e + t_u)$ in equation (A5) may be replaced with the equivalent terms from (A4). The expression for saturation count rate in terms of detector counts is, therefore:

$$A_s = \frac{\lambda[C(t_r) - C_{BG}]e^{\lambda t_u}}{\epsilon(1 - e^{-\lambda t_e})(1 - e^{-\lambda t_c})} \qquad (7)$$

where

$C(t_c) - C_{Bc}$ is C_{net}

as stated previously.

The geometry factor in detector counting efficiency was also calculated and verified for the G-M counter. It is true that the detector tube will only admit beta particles which are emitted in the direction of its window. The assumption is made that the collection of betas will be proportional to that part of the surface of a sphere included in the solid angle subtended by the window, where the center of the sphere is a point beta source. Certainly a flat foil is not a point source, but for the sake of simplicity it will be assumed to be so, then compared with experimental results to verify the assumption's validity. This geometry is depicted in two dimensions in figure A1.

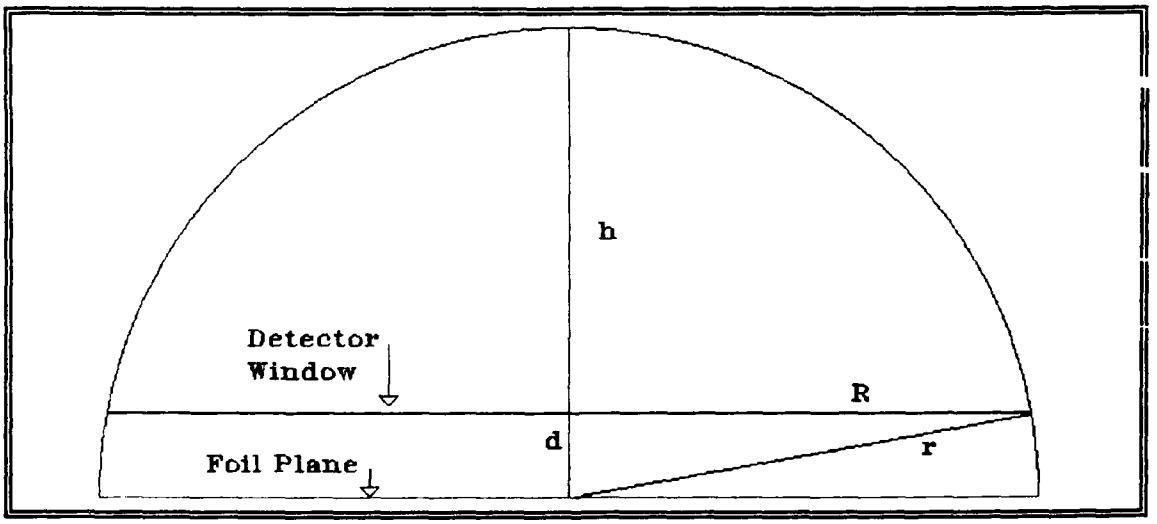

Figure A1. G-M Counter Collection Geometry

In figure A1 the dimensions indicated are:

-window diameter, R = 0.875"

-foil to window distance, d = 0.250"

-radius of the subtended sphere, r = 0.910"

-the apparent detector chamber depth, h = r - d.

The subtended angle of this detector is calculated from these dimensions to be 1.45π steradians.

In reality the foil is not an isotropic point source. A cosine correction must be applied because of the slab geometry (6:61). This correction is found using the following relation:

$$\text{cosine correction} = 1/2 \int_{-0.725\pi}^{0.725\pi} \cos\theta d\theta \qquad \text{(A6)}$$

A solution for (A6) using the dimensions of the G-M counter gives a cosine correction of 1.041. From these two contributions the value for the total correction is found to be $f_g = (1.45\pi)(1.041)/4\pi = 0.38$. Since the 2π counter had a geometry factor of 0.49, the ratio of the two constants is $f_g(\text{G-M})/f_g(2\pi) = 0.77$. Experimental data revealed an observed proportionality between the systems of 0.73. When this ratio is corrected for the estimated window absorption factor of the G-M counter, the experimental geometry dependent proportionality is equal to 0.76, a difference of 1.3% where counting statistics alone had an uncertainty of $\sigma \approx 1\%$.

The factors f_g, f_e and f_a are essentially independent of foil thickness. The other three counting corrections are not. In the Experimental Procedure and Results section, thickness dependent terms in ϵ are collectively represented as the product $f_v f_{bs} f_s$. It was stated that a cross-calibration curve was used to relate the counting efficiencies of detectors numbered 1 and 2. Equation (22) shows that:

$$(C_{s1}/C_{s2})e^{\mu_1 x} = (a_1/a_2)e^{\mu_2 x} \qquad \text{(A7)}$$

A least-squares fit was used to find the constants a_1/a_2 and μ_2. The count rates and the term μ_1 in equation (A7) were all known prior to making this calculation. Nine foils of differing thicknesses were

counted with each of the two proportional counter configurations so that a regression could be made on the adjusted ratio of count rates, $(C_{c1}/C_{c2})e^{\mu_2 x}$ as a function of foil thickness. The constants

$$a_1/a_2 = 0.927 \pm 0.028$$

and

$$\mu_2 = (1.04 \pm 0.11) \times 10^{-2} \text{ cm}^2/\text{mg}$$

are derived from this fit, which is represented graphically in figure A2.

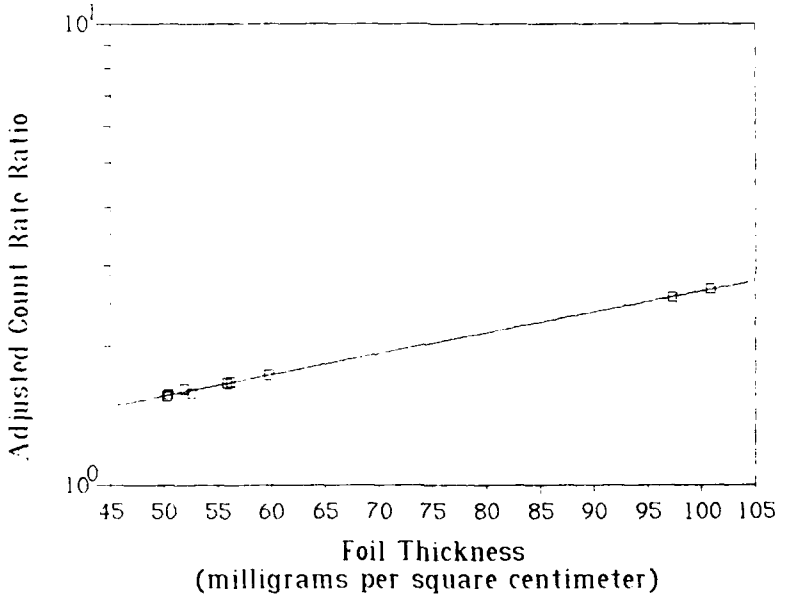

Figure A2. Ratio of Detector Saturation Count Rates, Adjusted for the Thickness Dependence of Count Rate In Detector #1, as a Function of Foil Thickness

The only other counting correction applies exclusively to cadmium-difference pairs. It is F_{Cd}, the correction for absorption of resonance neutrons in cadmium. For 0.030" Cd covers and the gold foils that were used for those irradiations, this correction is $F_{Cd} = 1.04 \pm 0.04$.

Appendix B: Pu-Be Source Strength Calculations

The three Pu-Be neutron sources used for detector calibrations were calibrated for neutron emission rate by the manufacturer at the times they were delivered. Due to the decay of trace amounts of ^{241}Pu (a beta emitter) to ^{241}Am (an alpha emitter) the strength of the two ^{239}Pu-Be sources is expected to increase over time, reaching a maximum approximately seventy years from the date of manufacture. Research conducted by Mound Laboratory over a thirteen year period confirms the predictability of these changes in source strength (24,25). The present day neutron emission by sources M580 and M1170 may be predicted by the equation (25:146):

$$Q(t) = Q(0)\left[1 + \frac{R}{(\lambda_3 - \lambda_4)}\left(e^{-\lambda_4 t} - e^{-\lambda_3 t}\right)\right] \qquad (B1)$$

where

$Q(t)$ is the source strength in $^{1}_{0}n/s$ at any time

$Q(0)$ is the source strength at the time of manufacture

R is the initial rate of increase in neutron yield (25:145).

From the Chart of the Nuclides, λ_3 and λ_4 are determined to be 0.0483/yr and 0.00160/yr respectively (3:47). For the experiments conducted from October through December of 1986 the values $t = 26.7$ yr for source M580 and $t = 24.6$ yr for source M1170 were used. Using this information and equation (B1) the present day source strengths are calculated directly to be:

$Q(t) = 1.05 \times 10^7$ $^{1}_{0}n/s$ for M580

$Q(t) = 1.10 \times 10^7$ $^{1}_{0}n/s$ for M1170

The SLAC source contains ^{238}Pu with negligible amounts of other radioisotopes. Its strength simply follows the decay of ^{238}Pu, with a half-life of 87.74 years. This source is reported to have had a strength of 2.04×10^7 $^1_0n/s$ when manufactured on 29 April, 1977. With decay over 9.70 years the strength of this source is calculated to be:

$$Q(t) = 1.92 \times 10^7 \ ^1_0n/s.$$

The three source strengths contained in this appendix were used in all phases of this study.

Appendix C: Pu-Be Source Anisotropy Correction

It was noted in the main body of this report that the flux from Pu-Be source M1170 is anisotropic and cylindrically symmetrical. For conditions where room-scattered neutrons are few in number this anisotropy will be described by the relation (26:F-5):

$$i(\theta) = \frac{A_s}{1/2 \int_0^{\pi} A_s(\theta')\sin\theta' d\theta'} \qquad (C1)$$

where

$i(\theta)$ is the anisotropy factor

A_s is the saturation activity for a foil irradiated by this particular source

θ is the orientation angle of the foil with respect to an axis perpendicular to the source's axis of cylindrical symmetry

θ' is a dummy variable of integration.

The denominator in equation (C1) is simply the average saturation activity of the foils, which is proportional to the average neutron flux from the source. This equation may be solved graphically for $i(\theta)$ after plotting $A_s(\theta)$ in polar coordinates. An alternate representation of the relationship between foil activity and orientation angle is given by the equation:

$$i(\theta) = \frac{A_s}{1/\pi \int_0^{\pi} A_s(\theta')d\theta'} \qquad (C2)$$

where

$A_s(\theta)$ is the ordinate in a rectangular coordinate system

θ is the abscissa in a rectangular coordinate system.

In fact, either relation yields the same result for $\iota(\theta)$ because both relations produce the unweighted mean value for $A_s(\theta)$. Equation (C2) is less intuitive, particularly when represented graphically, but far simpler to deal with numerically. This simplicity is the reason that it was chosen as the form for determining the anisotropy factor at $\theta = 90^\circ$.

A set of nine indium foils was used to determine $\iota(0)$. Each of the foils was activated separately in one of the flux integrators at each of three distances, 25 cm, 50 cm and 75 cm. The nine source orientation angles were from 0° to 180° in increments of 22.5°. Saturation activities were calculated in the usual manner and are represented graphically in figures C1 through C3. The mean activities were found by making a polynomial fit of the data and then calculating the mean ordinate analytically. The anisotropy factor at 90° is found from the ratio of the fitted value for $A_s(90^\circ)$ to the calculated mean.

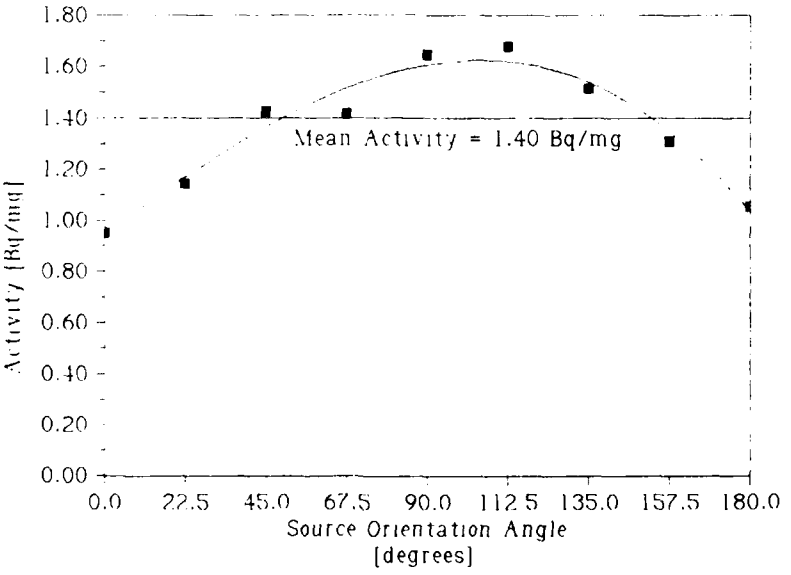

Figure C1. Foil Saturation Activity as a Function of Source Orientation Angle at a Source-to-Detector Distance of 25 cm

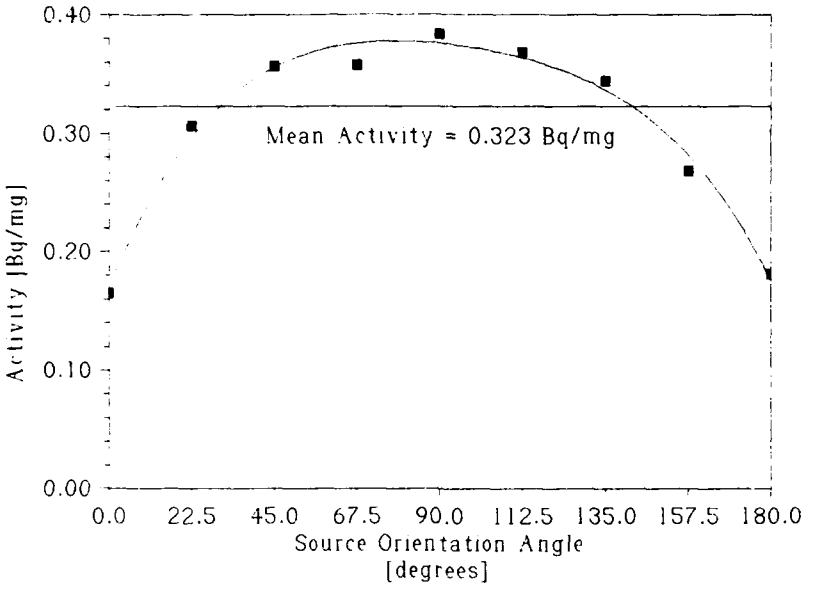

Figure C2. Foil Saturation Activity as a Function of Source Orientation Angle at a Source-to-Detector Distance of 50 cm

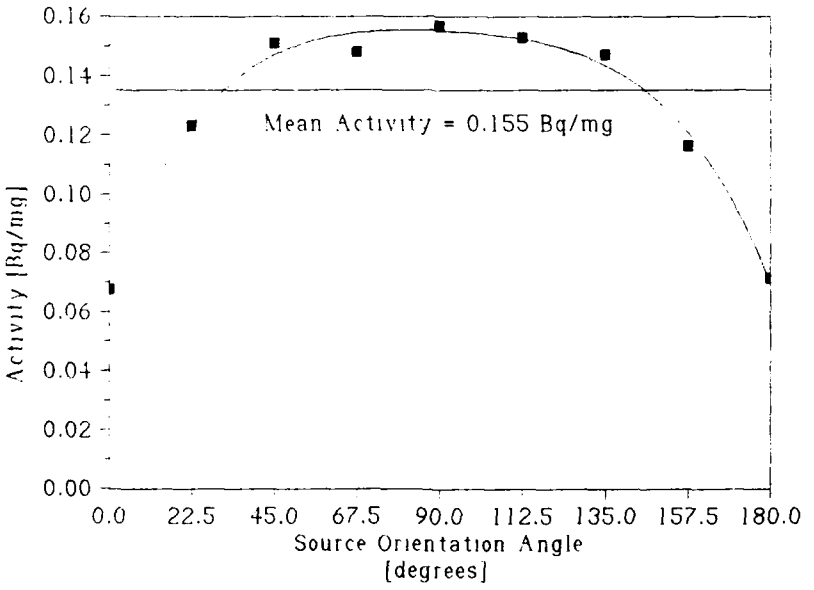

Figure C3. Foil Saturation Activity as a Function of Source Orientation Angle at a Source-to-Detector Distance of 75 cm

The polynomial functions that are plotted in the three figures are:

25 cm: $A_s(\theta) = 0.83 + (9.12 \times 10^{-3})\theta - (1.06 \times 10^{-5})\theta^2 - (2.09 \times 10^{-7})\theta^3$

50 cm: $A_s(\theta) = 0.149 + (6.76 \times 10^{-3})\theta - (9.23 \times 10^{-5})\theta^2 + (5.74 \times 10^{-7})\theta^3 - (1.49 \times 10^{-9})\theta^4$

75 cm: $A_s(\theta) = (6.82 \times 10^{-2}) + (3.41 \times 10^{-3})\theta - (5.06 \times 10^{-5})\theta^2 + (3.45 \times 10^{-7})\theta^3 - (9.36 \times 10^{-10})\theta^4$

The anisotropy factors which may be calculated from the three polynomials above are:

25 cm: $f(90°) = 1.15$

50 cm: $f(90°) = 1.16$

75 cm: $f(90°) = 1.15$

The value $f(90°) = 1.15$ was used as the anisotropy factor in all relevant calculations within this report. The results described above lead to the conclusion that for all practical purposes, neutron source M1170 behaves like an anisotropic point source.

Appendix D: Source Code Listing for FOIL5.BAS With Output

A source listing for FOIL5.BAS is included here. This code was compiled with the Microsoft QuickBasic compiler, version 4.00b. All of the saturation activity and thermal flux calculations were made using this program. In a few cases there are program lines which are more than seventy-two columns wide. They are wrapped in this listing, but to compile correctly, these lines must be continuous. This language syntax violation is obvious, and may be edited without any difficulty in the event that this listing must be transcribed to disk.

```
'*********************************************
'     This program calculates detector saturation count
'     rates, foil saturation activity, and thermal neutron
'     flux for gold or indium foils
'*********************************************
'     GLOSSARY OF VARIABLES:
'
'     Rs: saturation count rate as calculated for current
'       foil
'     lam: foil activation product decay constant
'     te(i): foil irradiation time
'     tw(i): wait time from the end of foil exposure to the
'       start of counting
'     tc(i): foil counting time
'     ctc(i): recorded number of counts in time tc
'     cnet(i): recorded number of counts in time tc
'     Qs(i): absolute disintegration rate of foil activation
'       products
'     ath: absolute disintegration rate due to thermal
'       neutrons
```

```
'     fg: counting system detector geometry factor
'     fw: detector window correction
'     fe: intrinsic counting efficiency
'     fgam: correction for photon induced reactions in alpha
'       or beta counting systems
'     fbs: correction for backscatter from foil backing
'       material
'     fs: correction for scatter and absorption within the
'       foil
'     n: number of foil irradiations in the data file listing
'     nl: number of foils in the data file listing
'     mass(i): foil mass
'     mass1: reference foil mass
'     thick(i): foil thickness in mg/cm**2
'     pi: the number pi
'     d(i): foil diameter
'     avog: Avogadro's number
'     z1,z2,z3,z4,z8: Temporary variables used to hold
'       intermediate results
'     rbg: Background count rate for the particular system
'     r0: Fractional remainder of activity from previous
'       irradiations
'     det(i): Detector ID number for a particular
'       irradiation
'     atomwt: Atomic weight of foil material
'     sig0!: Neutron absorption cross section of foil
'       material at .0253 eV
'     abund: Isotopic abundance of foil nuclide activated
'     fcd: Cd epithermal absorption correction for Cd
'       difference irradiations
'     F: Product of the six counting corrections
```

```
'     mass2: Cd covered foil mass.  Used in thermal flux
'       calculations
'     thick2: Cd covered foil thickness for thermal
'       flux calculations
'     Q: Actual saturation activity of a foil
'     errr: Percent standard deviation of saturation
'       count rate
'     era: Percent standard deviation of foil saturation
'       activity
'     ser1: Foil numerical serial number read from foil2.in
'     ser2: Foil numerical serial number read from foil1.in
'     ref: irradiation serial number reference.  Used to
'       identify foils with residual activity from a previous
'       irradiation
'     ty1: Foil type (a, b, c, d, or e) read from foil2.in
'     ty2: Foil type (a, b, c, d, or e) read from foil1.in
'     dummy: String variable containing response to prompt
'       for desire to calculate thermal flux
'     erbg1, erbg2, erbg3, erbg4: Percent standard deviation
'       of the background count rate for the various detector
'       configurations
'     k: Foil type specifier used when calculating equivalent
'       saturation count rates based on cross-calibration
'       constants
'     i: Loop counter
'     j: Loop counter used when associating foil serial
'       numbers with thickness during initial data read
'     k1: Type specifier used with k
'     i1, i2: Loop counters used to keep track of the two
'       foils during thermal flux calculations
'     FLUX: Calculated thermal flux
```

```
'     cadrat: Calculated Cd ratio
'     alf1, alf2: Self shielding/self absorption correction
'     erf: Percent standard deviation of the calculated
'       thermal flux
'     1: Temporary variable which hold detector type specifier
'     er0: Percent standard deviation calculated r0
'     gf: A correction which applies to some foil materials
'       which depart slightly from the usual 1/v thermal
'       absorption cross section dependance.  Indium is
'       an example with gf=1.011
'************************************************
'  Background count rates had these standard deviations
'     2pi counter                        -0.26%
'     G-M counter,  .329c/s rate         -0.71%
'     G-M counter,  .295c/s rate         -0.75%
'     G-M counter,  .281c/s rate         -0.50%
'  variable declarations

    DEFSTR D, T
    DEFINT N, R-S
    DIM Rs(3, 150) AS SINGLE, Qs(150), tc(150) AS SINGLE
    DIM erff(3) AS SINGLE, erff AS SINGLE
'   real cnet, z8
    DIM rbg(150) AS SINGLE, r0(150) AS SINGLE, te(150) AS SINGLE
    DIM tw(150) AS SINGLE, det(150) AS INTEGER, ctc(150), j AS INTEGER
'   real lam, massl, fgam, fs, atomwt, sig0!, abund, fcd, fg, fw, fe, F
    DIM mass2(150), thick2(150) AS SINGLE, mass(100), Q(150)
'   real fbs, avog
    DIM d(100) AS SINGLE, thick(100) AS SINGLE, errr(150), era(150)
'   real z1, z2, z3, z4
'   integer n,n1
```

```
    DIM ser(150), ser1(150), ser2(100), ref(150), F(3) AS SINGLE, F AS
SINGLE
    DIM ty1(150), ty2(100), dummy, k AS INTEGER, k1 AS INTEGER, i AS
INTEGER
'   set values for constants
      erbg1 = .0026
      erbg2 = .0071
      erbg3 = .0075
      erbg4 = .005
      fw = 1!
      fe = 1!
      Fcd = 1.04
      avog = 6.023E+23
'open data files
    OPEN "FOIL1.IN" FOR INPUT AS #1
    OPEN "FOIL2B.IN" FOR INPUT AS #2
    OPEN "FOIL.OUT" FOR OUTPUT AS #3

'read data from files
'   read irradiation data

    INPUT #2, n
    INPUT #1, n1
    FOR i = 1 TO n
        INPUT #2, ser(i)
        ty1(i) = INPUT$(1, #2)
        INPUT
#2,ser1(i),tc(i),ctc(i),rbg(i),r0(i),te(i),tw(i),det(i),ref(i)
    NEXT i
'   read file containing foil dimensions
    FOR i = 1 TO n1
```

```
        ty2(i) = INPUT$(1, #1)
        INPUT #1, ser2(i), mass(i), d(i), thick(i)
    NEXT i
'   write output file headers
    PRINT #3, "FOIL    IRRADIATION    RESULTS"
    PRINT #3, "SATURATION ACTIVITY CORRECTED FOR FOIL MASS."
    PRINT #3, ""
    PRINT #3, " SER DET   Rs1       Rs2       Rs3     %ERR     As/mg
As      %ERR"
    PRINT #3, "  #   #"
    PRINT #3, ""
'calculate saturation count rate (Rs) for each of the foils
    FOR i = 1 TO n
        FOR j = 1 TO n1
'       associate a foil mass and thickness with each irradiation
'       serial number
            IF (ty1(i) = ty2(j)) AND (ser1(i) = ser2(j)) THEN
                mass2(i) = mass(j)
                thick2(i) = thick(j)
                GOTO 50
            END IF
        NEXT j
'       determine counting corrections and foil constants based
'       on foil type
'       type a is 1/2"x.002" gold
50      SELECT CASE ty1(i)

            CASE "a"
                lam = LOG(2!) / (2.696 * 24! * 3600!)
                mass1 = 1!
'       type b is 1"x.002" indium
```

```
            CASE "b"
                mass1 = 1!
                lam = LOG(2!) / (54.1 * 60!)
                fgam = 1!
                fbs = 1!
'           this fs is only valid for thicknesses of 35 to 45 mg/cm2
'           in the 2pi counter with a thick silver backscatterer
                fs = .955 * EXP(-.00969 * thick2(i))
'       type c is 1"x.001" gold
            CASE "c"
                mass1 = 1!
                lam = LOG(2!) / (2.696 * 24! * 3600!)
'       type d foils are 1/2" and various thicknesses all normal-
'       ized to give count rates and activities per unit mass
'       of 1. mg
            CASE "d"
                mass1 = 1!
                lam = LOG(2!) / (2.696 * 24! * 3600!)
            CASE ELSE
                PRINT , "INVALID FOIL TYPE SPECIFIER.  EXECUTION
ABORTED!"
                GOTO 100
        END SELECT

            L = det(i)
'       calculate intermediate results for use in the saturation
'       count rate equation
        cnet = ctc(i) - rbg(i) * tc(i)
        z1 = EXP(lam * tw(i))
        z2 = 1! - EXP(-1! * lam * te(i))
        z3 = (1! - EXP(-1! * lam * tc(i))) / lam
```

```
'       calculate %standard deviation of Rs
        IF (rbg(i) = .585) THEN erbg = erbg1
        IF (rbg(i) = .329) THEN erbg = erbg2
        IF (rbg(i) = .295) THEN erbg = erbg3
        IF (rbg(i) = .281) THEN erbg = erbg4
        errr(i) = 100! * SQR(ctc(i) + (rbg(i) * tc(i) * erbg) ^ 2!) /
cnet
'       if this foil was previously irradiated, correct for Ro
        IF (Rs(L, ref(i)) = 0!) AND (ref(i) <> 0!) THEN
            PRINT #3, "serial*", ser(i), "invalid"
        END IF
        IF r0(i) <> 0! THEN
            z4 = (1! - EXP(-1! * lam * te(ref(i))))
            er0 = (errr(i) * cnet / 100!) ^ 2!
            z8 = Rs(L, ref(i)) * z4 * r0(i) * z3 * mass2(ref(i)) / z1
            cnet = cnet - z8
'       calculate %standard deviation of Rs for this case
            errr(i) = 100! * SQR(er0 + (errr(ref(i)) * z8 / 100!) ^ 2!)
/ cnet
        END IF
'       this statement combines all the intermediate results to
'       yield saturation count rate corrected to a standard foil
'       mass for the particular foil type code
        Rs(L, i) = cnet * z1 * mass1 / (z2 * z3 * mass2(i))
'       calculate Qs, the saturation activity normalized for
'       foil mass, and Q, the actual activity
'       F = fg * fs * fw * fe * fgam * fbs
        SELECT CASE ty1(i)
            CASE "a", "c", "d"
                F(1) = 1.138 * .49 * .927 * EXP(-.00986 * thick2(i))
                erff(1) = F(1) * SQR((thick2(i) * .00035 / EXP(-.00986 *
```

```
thick2(i))) ^ 2 + (.028 / 1.138) ^ 2)
                F(2) = 1.138 * .49 * EXP(-.0104 * thick2(i))
                erff(2) = F(2) * SQR((thick2(i) * .00037 / EXP(-.0104 *
thick2(i))) ^ 2 + (.028 / 1.138) ^ 2)
                F(3) = 1.138 * .38 * .943 * EXP(-.0104 * thick2(i))
                erff(3) = F(3) * SQR((thick2(i) * .00037 / EXP(-.0104 *
thick2(i))) ^ 2 + (.04 / .943) ^ 2 + (.028 / 1.138) ^ 2)
'       assign the standard deviation of the counting efficiency
                erff = erff(L)
            CASE "b"
                F(1) = .49 * .929 * fs
                F(2) = .49 * fs
                F(3) = .943 * .38 * fs
                erff = .02
'***CAUTION - BECAUSE OF THE DEPENDENCY ON DETECTOR CONFIGURATION
'             OF THE BACKSCATTER CORRECTION, THIS CONVERSION IS
'             ONLY VALID FOR A LIMITED RANGE OF FOIL THICKNESSES!***
        END SELECT
        F = F(L)
'       calculate Rs that would have been seen with the other two
'       detector configurations
        FOR k1 = 1 TO 3
            Rs(k1, i) = Rs(L, i) * F(k1) / F(L)
        NEXT k1
        Qs(i) = Rs(L, i) / F
        Q(i) = Qs(i) * mass2(i) / mass1
'       calculate the %uncertainty of the saturation activity
                era(i) = 100! * SQR((erff / F) ^ 2 + (errr(i) / 100!) ^
2!)
'       write results to output file
        PRINT #3, USING "###_   #_ ###.#####_ ###.#####_ ###.#####_
```

```
###.##_ ###.#####_ ####.####_ ###.##"; ser(i); L; Rs(1, i); Rs(2, i);
Rs(3, i); errr(i); Qs(i); Q(i); era(i)
    NEXT i

'   open the file which lists serial numbers for Cd-difference pairs
    OPEN "fluxes" FOR INPUT AS #5

    OPEN "flux.out" FOR OUTPUT AS #4
    PRINT #4, "ABSOLUTE DETERMINATION OF THERMAL FLUX"
    PRINT #4,
    PRINT #4, " SER  #'s     FLUX   Cd RATIO %ERROR %ERROR(neglecting
Fcd)"
    PRINT #4,

80 INPUT #5, i1, i2
    IF (i1 = 0!) GOTO 100

'   calculate cadmium ratio
    cadrat = Qs(i1) / (Qs(i2) * Fcd)
    IF tyl(i1) = "b" THEN
'   this is the data for indium
        atomwt = 115!
        sig0! = 1.45E-22
        abund = .9577
        gf = 1.011
'       calculate the thermal neutron self shielding correction
'       factor by linear interpolation from Greenfield's table.
        alf1 = .00143 * thick2(i1) + .974
        alf2 = .00143 * thick2(i2) + .974
    ELSE
'   this is the data for gold
```

```
        atomwt = 197!
        sig0! = 9.87E-23
        abund = 1!
        alf1 = 1!
        alf2 = 1!
        gf = 1!
    END IF
'   calculate the absolute thermal flux
    z1 = Q(i1) / (alf1 * mass2(i1))
    z2 = Q(i2) * Fcd / (alf2 * mass2(i2))
    z3 = 1.128 * 1000! * atomwt / (sig0! * avog * abund * gf)
    flux = (z1 - z2) * z3
'   calculate the %uncertainty in the result, first
'   incorporating the contribution to uncertainty due to
'   an assumed error in fcd of sigma = 0.0128
    erfcd = .0128 ^ 2!
    erf = 100! * SQR((z1 * era(i1) / 100!) ^ 2! + erfcd + (z2 * era(i2)
/ 100!) ^ 2!) / ABS(z1 - z2)
    erf1 = 100! * SQR((z1 * era(i1) / 100!) ^ 2! + (z2 * era(i2) / 100!)
^ 2!) / ABS(z1 - z2)
    PRINT #4, USING "_ ###_  ###_    #####._   ###.##_ ###.##_ ###.##";
i1; i2; flux; cadrat; erf; erf1
    GOTO 80
100    END
'*************************************************
'*************************************************
```

Foil Irradiation Data

Lists of foil dimensions and irradiation data (raw and processed) are provided here. The input data (foil dimensions and counting statistics) are know to be accurate but the calculated saturation activities have a large uncertainty. This tabulation may be of interest to anyone who attempts to refine the counting corrections used in FOIL5.BAS simply because it provides a large comparison data set.

Foil serial numbers have both a letter and number part. The letter indicates the foil's material and approximate dimensions. Foils beginning with "a" are 0.5 inch diameter, 0.002 inch thick gold; foils beginning with "b" are 1.0 inch diameter, 0.002 inch thick indium; foils beginning with "c" are 1.0 inch diameter, 0.001 inch thick gold; foils beginning with "d" and "e" are gold of various diameters and thicknesses. The number part of the serial number is merely a consecutive assignment without any special significance.

Foil Serial #	Mass [mg]	Diameter [cm]	Thickness [mg/cm^2]
a 01	125.1	1.281	97.1
a 02	131.1	1.277	102.4
a 03	134.9	1.287	103.7
a 04	130.1	1.288	99.9
a 05	135.9	1.279	105.8
a 06	135.3	1.288	103.8
a 07	132.2	1.288	101.5
a 08	128.8	1.288	98.9
a 09	134.0	1.290	102.5
a 10	130.9	1.288	100.5
a 11	131.5	1.291	100.5
a 12	132.6	1.289	101.6
a 13	133.2	1.284	102.9
a 14	129.6	1.286	99.8

Foil Serial #	Mass [mg]	Diameter [cm]	Thickness [mg/cm^2]
a 15	136.9	1.280	106.4
a 16	127.1	1.290	97.2
a 17	125.0	1.282	96.8
a 18	124.8	1.278	97.3
a 19	128.9	1.281	100.0
a 20	131.9	1.277	103.0
a 21	133.8	1.276	104.6
b 01	186.6	2.552	36.5
b 02	180.0	2.554	35.1
b 03	182.1	2.557	35.5
b 04	215.5	2.556	42.0
b 05	193.9	2.556	37.8
b 06	222.5	2.557	43.3
b 07	227.6	2.552	44.5
b 08	229.6	2.554	44.8
b 09	202.5	2.547	39.7
b 10	200.4	2.559	39.0
c 01	254.0	2.555	49.5
c 02	242.9	2.555	47.4
c 03	253.2	2.547	49.7
c 04	246.0	2.552	48.1
c 05	249.2	2.553	48.7
c 06	255.5	2.552	50.0
c 07	250.6	2.552	49.0
c 08	240.0	2.549	47.0
c 09	251.2	2.550	49.2
c 10	248.5	2.559	48.3
c 11	244.9	2.550	48.0
c 12	249.6	2.553	48.8
c 13	242.3	2.560	47.1

Foil Serial #	Mass [mg]	Diameter [cm]	Thickness [mg/cm^2]
c 14	245.3	2.553	47.9
c 15	291.6	2.546	57.3
c 16	259.6	2.548	50.9
c 17	273.3	2.557	53.2
c 18	278.0	2.551	54.4
c 19	267.4	2.554	52.2
c 20	256.8	2.550	50.3
c 21	286.4	2.555	55.9
c 22	257.3	2.549	50.4
c 23	287.6	2.552	56.2
c 24	265.9	2.554	51.9
c 25	278.7	2.566	53.9
c 26	271.9	2.566	52.6
c 27	271.9	2.541	53.6
c 28	300.7	2.547	59.0
c 29	279.0	2.560	54.2
c 30	281.0	2.555	54.8
d 01	31.2	1.284	24.1
d 02	77.3	1.283	59.8
d 03	129.8	1.280	100.9
d 04	32.0	1.285	24.7
d 05	73.0	1.280	56.7
d 06	125.2	1.280	97.3
d 07	102.3	1.128	102.4
d 08	102.1	1.125	102.7
d 09	102.1	1.121	103.4
d 10	101.2	1.125	101.8
d 11	100.5	1.125	101.1
d 12	101.6	1.120	103.1
d 13	101.4	1.126	101.8

Foil Serial #	Mass [mg]	Diameter [cm]	Thickness [mg/cm^2]
d 14	101.8	1.134	99.6
e 01	123.0	2.550	24.1
e 02	293.2	2.550	57.4
e 03	501.8	2.550	98.3
d 15	101.8	1.132	101.2

The following is a list of all foil counting data amassed for the preceding study. Most of the column headings are self-explanatory. Of those which are not, r_{bg} is the background count rate for the beta detector used, r_0 is the beta count rate which the foil is estimated to have from previous irradiations, and the reference count number is the count number of the foil's last irradiation (where zero indicates no prior irradiations).

Count Number	Foil Serial Number	t_c [s]	$C(t_c)$	r_{bg} [s^{-1}]	r_0 [s^{-1}]	t_e [s]	t_u [s]	Detector Number	Ref. Count #
4	b 1	400	11511	.585	.000	6540	720	1	0
5	b 1	400	10666	.585	.000	6540	1500	2	0
6	b 2	1000	9023	.585	.000	7140	720	1	0
7	b 2	2000	12781	.585	.000	7140	2220	2	0
8	b 3	2000	6397	.585	.000	4980	600	1	0
9	b 3	4000	8042	.585	.000	4980	2940	2	0
11	b 1	1000	14281	.585	.000	1800	600	1	0
12	b 2	1000	16708	.585	.000	1800	600	1	0
13	b 3	1000	20817	.585	.000	1800	600	1	0
14	b 4	1000	22920	.585	.000	1800	600	1	0
15	b 5	1000	24918	.585	.000	1800	600	1	0
16	b 6	1000	27561	.585	.000	1800	600	1	0
17	b 7	1000	25211	.585	.000	1800	600	1	0
18	b 8	1000	22020	.585	.000	1800	600	1	0
19	b 9	1000	16567	.585	.000	1800	600	1	0

Count Number	Foil Serial Number	t_c [s]	$C(t_c)$	r_{bg} [s^{-1}]	r_o [s^{-1}]	t_e [s]	t_u [s]	Detector Number	Ref. Count #
20	b 1	2000	5469	.585	.000	1800	600	1	0
21	b 2	2000	8976	.585	.000	1800	600	1	0
22	b 3	2000	10315	.585	.000	1800	600	1	0
23	b 4	2000	11360	.585	.000	1800	600	1	0
24	b 5	2000	11425	.585	.000	1800	600	1	0
25	b 6	2000	11873	.585	.000	1800	600	1	0
26	b 7	2000	11279	.585	.000	1800	600	1	0
27	b 8	2000	9104	.585	.000	1800	600	1	0
28	b 9	2000	6002	.585	.000	1800	720	1	0
29	c 2	8000	19059	.585	.000	66540	420	1	0
30	b 1	3000	5793	.585	.000	3600	600	1	0
31	b 2	3000	8917	.585	.000	3600	600	1	0
32	c 3	10000	12272	.585	.000	66120	600	1	0
33	b 3	3000	10611	.585	.000	3600	600	1	0
34	b 4	3000	11411	.585	.000	3600	600	1	0
35	b 5	3000	11339	.585	.000	3600	600	1	0
36	c 1	2000	16630	.585	.000	64320	300	1	0
37	b 6	3000	11915	.585	.000	3600	600	1	0
38	b 7	3000	11646	.585	.000	3600	600	1	0
39	b 8	3000	9618	.585	.000	3600	600	1	0
40	b 9	3000	6225	.585	.000	3600	600	1	0
41	c 4	20000	21360	.585	.000	72300	1200	1	0
42	c 5	15000	21572	.585	.000	240420	1020	1	0
43	c 6	15000	23201	.585	.000	593760	480	1	0
45	a 2	60000	42912	.585	.000	159000	2580	1	0
46	a 3	30000	27131	.585	.000	159000	68880	1	0
47	a 1	20000	12791	.585	.000	148380	2520	1	0
48	a 4	40000	38569	.585	.000	91860	1260	1	0
49	a 5	60000	48716	.585	.000	76860	2340	1	0

Count Number	Foil Serial Number	t_c [s]	$C(t_c)$	r_{bg} [s^{-1}]	r_o [s^{-1}]	t_e [s]	t_u [s]	Detector Number	Ref. Count #
50	a 6	50000	39881	.585	.000	91740	3300	1	0
51	a 7	4000	2393	.585	.000	102720	1860	1	0
52	c 10	8000	16472	.585	.000	56580	2700	1	0
53	c 11	8000	12316	.585	.000	81000	1020	1	0
54	c 12	8000	13269	.585	.000	72720	720	1	0
55	c 13	4000	10328	.585	.000	69960	480	1	0
56	c 14	3000	13922	.585	.000	178140	660	1	0
57	c 15	4000	22015	.585	.000	183000	8640	1	0
58	c 16	8000	26346	.585	.000	69780	360	1	0
59	c 17	2000	20674	.585	.000	67140	660	1	0
60	c 18	8000	15807	.585	.000	85560	840	1	0
61	c 19	10000	15756	.585	.000	89520	1080	1	0
62	c 17	2000	15967	.329	.000	67140	14640	3	0
63	c 18	8000	11505	.295	.000	85560	8940	3	0
64	c 20	20000	21151	.585	.000	76020	360	1	0
65	c 20	20000	13461	.295	.000	76020	20640	3	0
66	a 8	40000	12270	.281	.000	223500	23520	3	0
67	a 9	40000	26511	.585	.000	223500	23520	1	0
68	a 10	60000	24074	.281	.000	223500	111660	3	0
69	a 11	20000	21200	.585	.000	223500	540	1	0
70	a 12	20000	14293	.281	.000	223500	600	3	0
71	a 13	30000	17114	.281	.000	223500	64200	3	0
72	a 14	40000	33564	.585	.000	223500	64200	1	0
73	c 5	80000	56282	.585	.001	120	103440	1	2
74	c 11	4000	11613	.281	.132	1500	179160	3	3
75	c 12	4000	14255	.281	.129	1500	183360	3	4
76	c 1	20000	10130	.281	.000	1500	284760	3	6
77	c 13	20000	15470	.281	.162	1500	258180	3	5

Count Number	Foil Serial Number	t_c [s]	$C(t_r)$	r_{bg} [s-1]	r_0 [s-1]	t_e [s]	t_u [s]	Detector Number	Ref. Count #
78	c 2	60000	65207	.585	.000	1500	388620	1	9
79	c 14	40000	42385	.585	.224	1500	475980	1	6
80	a 15	20000	15474	.585	.000	1500	280620	1	0
81	a 16	20000	25362	.585	.000	1500	215760	1	0
82	a 17	4000	6763	.585	.000	1500	182520	1	0
83	a 18	4000	9482	.585	.000	1500	177600	1	0
84	a 19	4000	7165	.585	.000	1500	173280	1	0
85	a 20	6000	8150	.585	.000	1500	186960	1	0
86	a 21	20000	18175	.585	.000	1500	254400	1	0
87	c 17	4000	16632	.281	.355	1500	181620	3	2
88	c 18	6000	11220	.281	.459	1500	186900	3	3
89	c 16	80000	56102	.281	.358	1500	385080	3	8
90	c 3	30000	26526	.585	.000	1500	317280	1	2
91	c 15	30000	43166	.585	.278	1500	351300	1	7
92	c 4	30000	12550	.281	.000	1500	317160	3	1
93	c 8	20000	34325	.585	.000	232980	634080	1	0
94	c 9	50000	28023	.281	.000	232980	633960	3	0
95	c 7	40000	59364	.281	.000	68400	734220	3	0
96	c 19	400	8429	.281	.097	315120	3180	3	1
97	c 19	20000	399168	.281	.097	315120	4740	3	1
98	c 20	400	17658	.281	.123	315060	1020	3	5
99	c 20	400	17781	.281	.123	315060	2820	3	5
100	c 20	200	11454	.585	.123	315060	5400	2	4
101	c 20	200	10865	.585	.123	315060	5820	1	4
102	c 21	400	36223	.281	.000	315000	3420	3	0
103	c 21	400	50110	.585	.000	315000	1080	2	0
104	c 21	400	47769	.585	.000	315000	1620	1	0
105	c 21	400	49590	.585	.000	315000	2280	2	0
106	c 22	400	80643	.585	.000	313920	3960	2	0

Count Number	Foil Serial Number	t_c [s]	$C(t_c)$	r_{bg} [s^{-1}]	r_0 [s^{-1}]	t_e [s]	t_u [s]	Detector Number	Ref. Count #
107	c 22	400	57791	.281	.000	313920	360	3	0
108	c 22	400	78811	.585	.000	313920	840	1	0
109	c 22	400	83202	.585	.000	313920	1560	2	0
110	c 23	200	36171	.585	.000	313740	4920	1	0
111	c 23	400	53689	.281	.000	313740	660	3	0
112	c 23	200	37316	.585	.000	313740	7440	2	0
113	c 24	400	27651	.281	.000	314880	600	3	0
114	c 24	200	17659	.585	.000	314880	4680	1	0
115	c 24	200	18226	.585	.000	314880	5100	2	0
116	c 26	400	28043	.585	.000	339660	540	1	0
117	c 26	400	29450	.585	.000	339660	6120	2	0
118	c 26	400	29167	.585	.000	339660	6720	2	0
119	c 25	400	13401	.585	.000	338400	3600	1	0
120	c 27	400	26529	.585	.000	339600	1140	1	0
121	c 28	800	19042	.585	.000	338400	2460	1	0
122	c 29	2000	10313	.585	.000	338400	3900	1	0
123	c 30	20000	18370	.281	.000	338400	8220	3	0
125	d 1	300	10489	.585	.000	355200	720	1	0
128	d 1	300	11205	.585	.000	355200	2220	2	0
131	d 4	300	12107	.585	.000	355200	3900	2	0
142	d 7	1000	21847	.585	.000	340800	900	1	0
143	d 8	1000	14234	.585	.000	340380	4920	1	0
144	d 9	2000	13349	.585	.000	340320	6480	1	0
145	d 10	2000	6358	.585	.000	340140	11760	1	0
146	d 11	1000	7997	.585	.000	609480	23460	1	0
147	d 12	3000	5021	.585	.000	609420	14640	1	0
148	d 13	4000	2956	.585	.000	609420	9840	1	0
149	d 14	4000	2038	.585	.000	609300	840	1	0

The following data is a listing of the output from FOIL5.BAS. The count numbers are grouped according to similarities in the way the output was used. A brief description of the particular use or irradiation conditions precedes each group. The three columns headed by C_{s1}, C_{s2}, and C_{s3} respectively include the *saturation count rates* for each of the three beta counters. One of the three for each count is the actual C_s, while the other two values are expected count rates from the two counters that were not used. These expected values are calculated using the ratio of the total counting efficiency factors for the counters as a cross-calibration factor.

Counts 4 through 9 come from three foils, each counted in two beta counters after an irradiation. This set is used in determining the cross-calibration factor between counters 1 and 2.

Count Number	Detector Number	C_{s1}	C_{s2}	C_{s3}	$\%\sigma_{C_s}$	A_s/mg	A_s	$\%\sigma_{A_s}$
4	1	0.24427	0.26294	0.19229	0.95	0.80032	149.33	6.62
5	2	0.24797	0.26692	0.19520	0.99	0.81244	151.60	6.17
6	1	0.07761	0.08354	0.06109	1.13	0.25084	45.15	6.56
7	2	0.07560	0.08138	0.05951	0.97	0.24436	43.98	6.08
8	1	0.03062	0.03296	0.02410	1.53	0.09934	18.08	6.67
9	2	0.03095	0.03331	0.02436	1.58	0.10041	18.28	6.23

Counts 11 through 19 are from indium foils irradiated with source M1170. These are foils that were activated 25 cm from the source in a flux integrator. The source orientation angle was varied from 0° to 180° in 22.5° increments. The counts are listed in order of orientation angle from smallest to largest.

Count Number	Detector Number	C_{s1}	C_{s2}	C_{s3}	$\%\sigma_{C_s}$	A_s/mg	A_s	$\%\sigma_{A_s}$
11	1	0.29035	0.31254	0.22856	0.87	0.95127	177.50	6.61
12	1	0.35433	0.38141	0.27893	0.80	1.14526	206.14	6.51
13	1	0.43950	0.47309	0.34598	0.71	1.42607	259.68	6.53

Count Number	Detector Number	C_{s1}	C_{s2}	C_{s3}	$\%\sigma_{C_s}$	A_s/mg	A_s	$\%\sigma_{A_s}$
14	1	0.40999	0.44132	0.32274	0.68	1.41679	305.31	6.94
15	1	0.49642	0.53436	0.39078	0.65	1.64706	319.36	6.67
16	1	0.47960	0.51626	0.37754	0.62	1.67836	373.43	7.03
17	1	0.42801	0.46072	0.33693	0.64	1.51534	344.89	7.11
18	1	0.36930	0.39753	0.29072	0.69	1.31130	301.07	7.14
19	1	0.31220	0.33607	0.24577	0.81	1.05510	213.65	6.81

The following nine counts are from indium foils irradiated with source M1170. These are foils that were activated 50 cm from the source in a flux integrator. The source orientation angle was varied from 0° to 180° in 22.5° increments. The counts are listed in order of orientation angle from smallest to largest.

Count Number	Detector Number	C_{s1}	C_{s2}	C_{s3}	$\%\sigma_{C_s}$	A_s/mg	A_s	$\%\sigma_{A_s}$
20	1	0.05041	0.05427	0.03969	1.72	0.16518	30.82	6.78
21	1	0.09490	0.10215	0.07470	1.21	0.30673	55.21	6.58
22	1	0.10989	0.11829	0.08651	1.11	0.35658	64.93	6.58
23	1	0.10347	0.11138	0.08145	1.05	0.35757	77.05	6.99
24	1	0.11573	0.12458	0.09111	1.04	0.38399	74.45	6.72
25	1	0.10526	0.11331	0.08286	1.02	0.36837	81.96	7.07
26	1	0.09719	0.10462	0.07651	1.05	0.34411	78.31	7.16
27	1	0.07562	0.08140	0.05953	1.20	0.26850	61.64	7.20
28	1	0.05357	0.05767	0.04217	1.60	0.18105	36.66	6.95

The following nine counts are from indium foils irradiated with source M1170. These are foils that were activated 75 cm from the source in a flux integrator. The source orientation angle was varied from 0° to 180° in 22.5° increments. The counts are listed in order of orientation angle from smallest to largest.

Count Number	Detector Number	C_{s1}	C_{s2}	C_{s3}	$\%\sigma_{C_s}$	A_s/mg	A_s	$\%\sigma_{A_s}$
30	1	0.02070	0.02228	0.01630	1.89	0.06782	12.65	6.82
31	1	0.03806	0.04097	0.02996	1.32	0.12303	22.14	6.60
33	1	0.04652	0.05008	0.03662	1.16	0.15095	27.48	6.59
34	1	0.04286	0.04614	0.03374	1.11	0.14812	31.92	7.00
35	1	0.04728	0.05090	0.03722	1.11	0.15688	30.41	6.73
37	1	0.04368	0.04702	0.03439	1.08	0.15286	34.01	7.08
38	1	0.04157	0.04475	0.03273	1.09	0.14718	33.49	7.16
39	1	0.03276	0.03526	0.02579	1.25	0.11632	26.70	7.21
40	1	0.02112	0.02273	0.01662	1.77	0.07136	14.45	6.99

This next group of counts is from gold foils irradiated with source M1170 under low-scatter conditions in the a flux integrator. Count 36 is from an irradiation at 25 cm. Counts numbered 29, 52, 55, 56, and 57 are all from 50-*cm* irradiations. The rest of the counts are from irradiations at distances from 75 cm to 150 cm consecutively in 25 cm increments.

Count Number	Detector Number	C_{s1}	C_{s2}	C_{s3}	$\%\sigma_{C_s}$	A_s/mg	A_s	$\%\sigma_{A_s}$
36	1	0.17538	0.18420	0.13471	0.83	0.55276	140.40	3.84
29	1	0.04174	0.04389	0.03209	0.96	0.12885	31.29	3.74
52	1	0.03905	0.04104	0.03001	1.09	0.12162	30.22	3.83
55	1	0.04418	0.04646	0.03398	1.27	0.13598	32.94	3.82
56	1	0.04044	0.04251	0.03109	0.97	0.12547	30.77	3.77
57	1	0.04146	0.04337	0.03171	0.75	0.14113	41.15	4.37
32	1	0.01444	0.01516	0.01109	1.74	0.04560	11.54	4.14
41	1	0.01049	0.01102	0.00806	1.55	0.03259	8.01	3.97
42	1	0.00687	0.00722	0.00528	1.16	0.02148	5.35	3.87
43	1	0.00465	0.00488	0.00357	1.07	0.01472	3.76	3.92

Counts numbered 53 and 54 are from gold foil irradiations in a flux integrator at 50 cm under low-scatter conditions. Source M1170 was used. The source orientation angles were 0° and 180° respectively.

Count Number	Detector Number	C_{s1}	C_{s2}	C_{s3}	$\%\sigma_{C_s}$	A_s/mg	A_s	$\%\sigma_{A_s}$
53	1	0.01847	0.01942	0.01420	1.46	0.05736	14.04	3.93
54	1	0.02242	0.02355	0.01723	1.35	0.07017	17.51	3.94

The next seven counts are from Bonner sphere irradiations under low-scatter conditions at source-to-foil distances of 75 cm. Source M1170 was used. The counts are listed in order of sphere size, from smallest to largest, with count 51 being from a bare foil irradiation.

Count Number	Detector Number	C_{s1}	C_{s2}	C_{s3}	$\%\sigma_{C_s}$	A_s/mg	A_s	$\%\sigma_{A_s}$
51	1	0.00038	0.00039	0.00029	93.01	0.00203	0.26	93.54
47	1	0.00127	0.00130	0.00095	10.73	0.00639	0.79	14.13
45	1	0.00290	0.00296	0.00216	2.90	0.01539	2.01	10.55
46	1	0.00806	0.00822	0.00601	1.78	0.04334	5.84	10.54
48	1	0.01298	0.01326	0.00970	1.36	0.06722	8.74	9.78
49	1	0.00898	0.00915	0.00669	1.75	0.04931	6.70	10.94
50	1	0.00715	0.00729	0.00533	2.01	0.03849	5.20	10.60

The following eight counts are from gold foil irradiations with source M1170 under high-scatter conditions. The foils were irradiated in flux integrators at distances of 25 cm to 125 cm in 25 cm increments. The counts are listed in order of increasing source-to-foil distance with the exception of counts 64 and 65, which were *both* at 125 cm.

Count Number	Detector Number	C_{s1}	C_{s2}	C_{s3}	$\%\sigma_{C_s}$	A_s/mg	A_s	$\%\sigma_{A_s}$
59	1	0.19801	0.20755	0.15179	0.74	0.64726	176.89	4.06
62	3	0.21137	0.22155	0.16202	0.83	0.69092	188.82	6.04
58	1	0.05636	0.05915	0.04326	0.75	0.18011	46.75	3.91
60	1	0.02258	0.02365	0.01730	1.14	0.07469	20.76	4.24
63	3	0.02482	0.02600	0.01901	1.19	0.08209	22.82	6.17
61	1	0.01613	0.01692	0.01237	1.28	0.05221	13.96	4.13
64	1	0.00937	0.00984	0.00720	1.57	0.02977	7.64	4.11
65	3	0.01037	0.01089	0.00796	1.64	0.03295	8.46	6.05

The next seven counts are from Bonner sphere irradiations under high-scatter conditions at source-to-foil distances of 100 cm. Source M1170 was used. The counts are listed in order of sphere size, from smallest to largest, with count 66 being from a bare foil irradiation.

Count Number	Detector Number	C_{s1}	C_{s2}	C_{s3}	$\%\sigma_{C_s}$	A_s/mg	A_s	$\%\sigma_{A_s}$
66	3	0.00063	0.00064	0.00047	12.06	0.00321	0.41	16.56
67	1	0.00136	0.00139	0.00101	5.59	0.00722	0.96	11.59
68	3	0.00385	0.00394	0.00288	2.45	0.02007	2.62	11.91
69	1	0.00767	0.00784	0.00573	1.57	0.03998	5.25	9.91
70	3	0.00930	0.00950	0.00695	1.42	0.04901	6.49	11.96
71	3	0.00759	0.00774	0.00566	1.58	0.04048	5.39	12.24
72	1	0.00518	0.00530	0.00387	1.90	0.02682	3.47	9.85

The following group of counts is from the Miami Valley Hospital experiments. These are all of the cadmium-difference pairs from that series of tests.

Count Number	Detector Number	C_{s1}	C_{s2}	C_{s3}	$\%\sigma_{C_s}$	A_s/mg	A_s	$\%\sigma_{A_s}$
76	3	0.62106	0.65230	0.47703	2.33	1.95742	497.18	6.23
77	3	1.01438	1.06678	0.78014	1.72	3.12228	756.52	5.93
78	1	0.75920	0.79829	0.58379	1.54	2.34376	569.29	3.93
79	1	1.06040	1.11469	0.81518	2.17	3.28976	806.97	4.24
90	1	0.71277	0.74854	0.54741	1.88	2.25089	569.92	4.20
91	1	0.86616	0.90590	0.66249	2.10	2.94814	859.67	4.79
92	3	0.43776	0.46012	0.33649	2.91	1.36077	334.74	6.41
89	3	0.82446	0.86528	0.63278	1.76	2.63460	683.94	6.11

The following counts are from gold foil irradiations at Miami Valley Hospital. These foils were exposed in flux integrators at radial distances from the x ray beam axis of 20 cm, 30 cm, 50 cm, and 100 cm. The counts are listed in such an order.

Count Number	Detector Number	C_{s1}	C_{s2}	C_{s3}	$\%\sigma_{C_s}$	A_s/mg	A_s	$\%\sigma_{A_s}$
74	3	5.24409	5.51231	4.03118	1.05	16.28526	3988.26	5.81
75	3	6.54503	6.87681	5.02905	0.93	20.48622	5113.36	5.82
87	3	4.12336	4.32210	3.16078	1.57	13.47854	3683.68	6.18
73	1	2.02380	2.12651	1.55513	2.83	6.32835	1577.02	4.65
88	3	2.37235	2.48509	1.81736	1.41	7.84711	2181.49	6.21

The next seven counts are from Bonner sphere irradiations at Miami Valley Hospital. The radial distance from the x ray beam axis was 20 cm. The counts are listed in order of sphere size, from smallest to largest, with count 80 being from a bare foil irradiation.

Count Number	Detector Number	C_{s1}	C_{s2}	C_{s3}	$\%\sigma_{C_s}$	A_s/mg	A_s	$\%\sigma_{A_s}$
80	1	0.73480	0.74840	0.54731	3.39	4.05853	555.61	11.43
81	1	2.36220	2.41791	1.76824	1.19	11.91577	1514.49	9.28
82	1	3.43946	3.52135	2.57518	1.86	17.28159	2160.19	9.33
83	1	5.48189	5.61089	4.10328	1.37	27.67992	3454.45	9.32
84	1	3.53986	3.61789	2.64578	1.76	18.35620	2366.11	9.86
85	1	2.31682	2.36405	1.72885	1.96	12.37471	1632.22	10.44
86	1	1.19307	1.21634	0.88952	2.13	6.47382	866.19	10.77

These three counts are from McCall's irradiations of gold foils with the SLAC source. The foils were exposed in flux integrators manufactured at AFIT. The source-to-foil distances were 25 cm, 50 cm, and 100 cm, with the counts listed in this order.

Count Number	Detector Number	C_{s1}	C_{s2}	C_{s3}	$\%\sigma_{C_s}$	A_s/mg	A_s	$\%\sigma_{A_s}$
95	3	0.31992	0.33610	0.24579	0.52	1.00335	251.43	5.78
93	1	0.06407	0.06738	0.04927	0.83	0.19700	47.28	3.69
94	3	0.02056	0.02160	0.01579	1.30	0.06460	16.22	5.91

Counts numbered 96 and 97 are from the same irradiation of a bare gold foil in the AFIT graphite pile at location FS6.

Count Number	Detector Number	C_{s1}	C_{s2}	C_{s3}	$\%\sigma_{C_s}$	A_s/mg	A_s	$\%\sigma_{A_s}$
96	3	0.16769	0.17587	0.12861	1.11	0.54277	145.13	6.03
97	3	0.16412	0.17213	0.12588	0.16	0.53123	142.05	5.93

Counts numbered 98 through 101 are from the same irradiation of a bare gold foil in the AFIT graphite pile at location FS5.

Count Number	Detector Number	C_{s1}	C_{s2}	C_{s3}	$\%\sigma_{C_s}$	A_s/mg	A_s	$\%\sigma_{A_s}$
98	3	0.36658	0.38485	0.28144	0.76	1.16450	299.04	5.87
99	3	0.37114	0.38963	0.28494	0.76	1.17898	302.76	5.87
100	2	0.35090	0.36839	0.26941	0.95	1.11470	286.25	4.10
101	1	0.34969	0.36712	0.26847	0.97	1.11084	285.26	3.92

Counts numbered 102 through 105 are from the same irradiation of a bare gold foil in the AFIT graphite pile at location FS4.

Count Number	Detector Number	C_{s1}	C_{s2}	C_{s3}	$\%\sigma_{C_s}$	A_s/mg	A_s	$\%\sigma_{A_s}$
102	3	0.68426	0.71620	0.52376	0.53	2.29708	657.88	6.17
103	2	0.68636	0.71840	0.52537	0.45	2.30414	659.90	4.47
104	1	0.68578	0.71779	0.52492	0.46	2.30218	659.34	4.22
105	2	0.68164	0.71345	0.52175	0.45	2.28827	655.36	4.47

Counts numbered 106 through 109 are from the same irradiation of a bare gold foil in the AFIT graphite pile at location FS3.

Count Number	Detector Number	C_{s1}	C_{s2}	C_{s3}	$\%\sigma_{C_s}$	A_s/mg	A_s	$\%\sigma_{A_s}$
106	2	1.24118	1.30297	0.95287	0.35	3.94672	1015.49	4.01
107	3	1.20446	1.26442	0.92468	0.42	3.82996	985.44	5.84
108	1	1.26152	1.32432	0.96849	0.36	4.01139	1032.13	3.82
109	2	1.27156	1.33487	0.97620	0.35	4.04334	1040.35	4.01

Counts numbered 110 through 112 are from the same irradiation of a bare gold foil in the AFIT graphite pile at location FS2.

Count Number	Detector Number	C_{s1}	C_{s2}	C_{s3}	$\%\sigma_{C_s}$	A_s/mg	A_s	$\%\sigma_{A_s}$
110	1	1.04840	1.09715	0.80235	0.53	3.52991	1015.20	4.25
111	3	1.00532	1.05207	0.76938	0.43	3.38486	973.48	6.18
112	2	1.04140	1.08983	0.79700	0.52	3.50637	1008.43	4.50

Counts numbered 113 through 115 are from the same irradiation of a bare gold foil in the AFIT graphite pile at location FS1.

Count Number	Detector Number	C_{s1}	C_{s2}	C_{s3}	$\%\sigma_{C_s}$	A_s/mg	A_s	$\%\sigma_{A_s}$
113	3	0.55629	0.58351	0.42673	0.60	1.79526	477.35	5.94
114	1	0.55012	0.57704	0.42200	0.76	1.77535	472.06	3.98
115	2	0.54209	0.56861	0.41583	0.75	1.74942	465.17	4.18

Counts numbered 116 through 118 are from the same irradiation of a cadmium covered gold foil in the AFIT graphite pile at location FS2.

Count Number	Detector Number	C_{s1}	C_{s2}	C_{s3}	$\%\sigma_{C_s}$	A_s/mg	A_s	$\%\sigma_{A_s}$
116	1	0.40288	0.42244	0.30893	0.60	1.30919	355.96	4.00
117	2	0.41043	0.43035	0.31472	0.59	1.33372	362.63	4.21
118	2	0.40718	0.42695	0.31223	0.59	1.32316	359.76	4.21

Counts numbered 119 through 123 are from irradiations of cadmium covered gold foils in the AFIT graphite pile. They were exposed at stringer locations FS1, FS3, FS4, FS5, and FS6, and are listed in that order.

Count Number	Detector Number	C_{s1}	C_{s2}	C_{s3}	$\%\sigma_{C_s}$	A_s/mg	A_s	$\%\sigma_{A_s}$
119	1	0.18821	0.19721	0.14422	0.88	0.61949	172.65	4.14
120	1	0.38167	0.39998	0.29251	0.62	1.25254	340.56	4.07
121	1	0.12269	0.12821	0.09376	0.74	0.42467	127.69	4.50
122	1	0.02620	0.02744	0.02007	1.11	0.08648	24.12	4.22
123	3	0.00493	0.00516	0.00377	1.09	0.01636	4.59	6.17

Counts numbered 142 through 145 are from irradiations of bare gold foils in the AFIT graphite pile. They were exposed at stringer locations FS1, FS5, FS6, and FS7, and are listed in that order.

Count Number	Detector Number	C_{s1}	C_{s2}	C_{s3}	$\%\sigma_{C_s}$	A_s/mg	A_s	$\%\sigma_{A_s}$
142	1	0.32750	0.33428	0.24446	0.70	1.73893	177.89	10.16
143	1	0.21333	0.21772	0.15922	0.87	1.13610	115.99	10.23
144	1	0.09577	0.09770	0.07145	0.95	0.51357	52.43	10.37
145	1	0.04182	0.04271	0.03123	1.54	0.22077	22.34	10.15

Counts numbered 146 through 149 are from irradiations of cadmium covered gold foils in the AFIT graphite pile. They were exposed at stringer locations FS1, FS5, FS6, and FS7, and are listed in that order.

Count Number	Detector Number	C_{s1}	C_{s2}	C_{s3}	$\%\sigma_{C_s}$	A_s/mg	A_s	$\%\sigma_{A_s}$
146	1	0.09463	0.09666	0.07069	1.21	0.49607	49.85	9.97
147	1	0.01343	0.01371	0.01002	2.17	0.07182	7.29	10.50
148	1	0.00188	0.00192	0.00140	8.88	0.00992	1.00	13.40
149	1	0.00000	0.00000	0.00000	15.08	0.00000	0.00	17.89

The following listing gives the results of FOIL5.BAS calculations for thermal neutron flux using cadmium-difference pairs.

Bare Foil Count Number	Cd Covered Foil Count Number	Experimental Flux [$\frac{1}{0}$n/cm²-s]	Calculated Flux [$\frac{1}{0}$n/cm²-s]	F_{Cd}	$\%\sigma_0$	Pile Stringer Number
115	119	4131	3844	2.72	7.14	FS1
112	118	7963	8235	2.55	7.91	FS2
106	120	9884	9425	3.03	6.33	FS3
105	121	6903	6807	5.18	5.68	FS4
100	122	3831	3784	12.39	4.65	FS5
97	123	1922	1749	31.22	6.61	FS6
77	76	4062	----	1.53	20.68	---

Bare Foil Count Number	Cd Covered Foil Count Number	Experimental Flux [$^{1}_{0}$n/cm^2-s]	Calculated Flux [$^{1}_{0}$n/cm^2-s]	F_{Cd}	$\%\sigma_\phi$	Pile Stringer Number
91	90	2270	----	1.26	28.41	---
89	92	4558	----	1.86	15.20	---
79	78	3186	----	1.35	19.91	---
142	146	4572	3829	3.37	15.09	FS1
143	147	3968	3769	15.21	11.04	FS5
144	148	1881	1742	49.77	10.89	FS6
145	149	843	767	45.98	11.44	FS7

Appendix E: Detector Configurations and Adjustments

Two beta counting systems were used for all experiments. The first of these systems is a windowless 2π proportional flow counter. This counter was used with both silver and steel backscatterers. The configurations, referred to as counter #2 and counter #1 respectively, are otherwise identical. A block diagram of this beta counter is presented in figure E1.

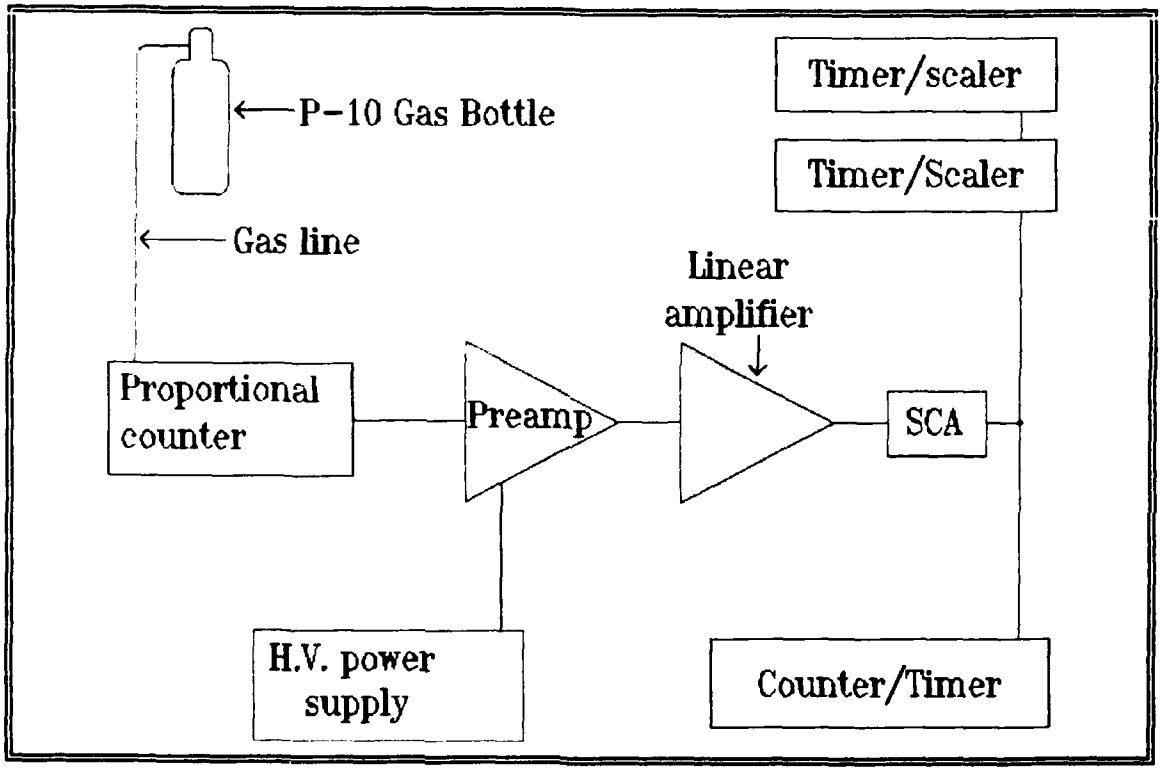

Figure E1. 2π Counter Block Diagram

The make and model of the components of the 2π counter, as well as the settings used are:

Nomenclature	Manufacturer	Model	Setting
Proportional Counter	NMC	PCC-10	
Charge Sensitive Preamp.	Canberra	2006	(fixed)

Nomenclature	Manufacturer	Model	Setting
Linear Amplifier	ORTEC	485	Coarse Gain: 8 Fine Gain: 6.75 Input: positive Output: unipolar
Single Channel Analyzer	Tennelec	TC441	LLD: 0.20 V Mode: E (LLD only)
Timer/Scaler	Tennelec	TC562P	
Timer/Scaler	Tennelec	TC562P	
Counter/Timer	Canberra	1772	
P-10 Gas	Matheson	---	3 psig
NIM Bin	Tennelec	527	
H. V. Power Supply	ORTEC	456	1,650 V

The G-M counter that was used is depicted in figure E2.

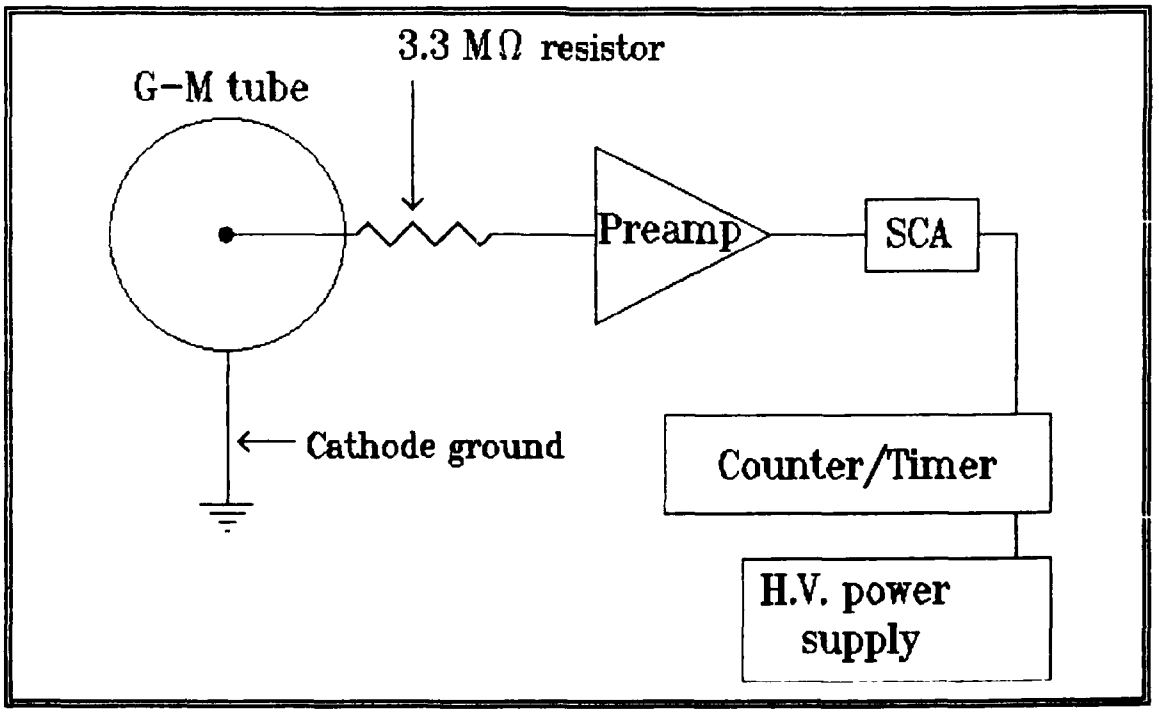

Figure E2. G-M Counter Block Diagram

The make and model of the components of the G-M counter, as well as the settings used are:

Nomenclature	Manufacturer	Model	Setting
G-M Tube	TGM	N1002	
3.3MΩ Resistor	---	----	
Preamplifier	Hewlett Packard	5554A	Shaped Pulse Output Voltage Gain: 2x Charge Sensitivity: 3 mV/pC
TSCA	Tennelec	TC444	
Counter/Timer	Canberra	1772	
H.V. Power Supply	Power Design	AEC-315B	850 V
NIM Bin	ORTEC	401A	

Appendix F: Ground Scatter Correction for Point Neutron Sources

In the process of calibrating the Bonner Sphere set and 6" moderators, it was necessary to make estimates of neutron flux under conditions where there was a lot of neutron scattering. If the average energy and neutron emission rate of a source is known, a simple means is available to estimate the scatter component of flux from a concrete plane. This simple recipe is explained in detail by T.M. Jenkins who found that it agreed with the more complex Monte Carlo calculations to within less than 10% (20:43).

Jenkins' method approximates the ground scatter contribution with an average energy dependent specular reflection model. The ratio of total to direct flux is given by the following equation (distances in cm):

$$\Phi_{total}/\Phi_{direct} = 1 + \frac{1.52 r_i / r_0}{[1 + 0.1E][1 + (r_i/r_0)^3]} \qquad (F1)$$

where

r_i is the distance travelled by scattered neutrons if they are assumed to undergo specular reflection

r_0 is the distance between the neutron source and detector

E is the average neutron energy

In the case of the 6" moderator, the source and foil heights above the scattering plane were both 25 cm. For the Bonner Sphere set the source height was 25 cm and the detector heights were all 15 cm. A value of $E = 4.2$ MeV was used in both cases. The resulting ratios of total to direct fluence are shown in table F.

Table F

Ratios of Total to Direct Flux for Foil Irradiations Conducted Under Conditions Where There Was Significant Neutron Scattering From a Concrete Plane

r_0 [cm]	r_i [cm]	$\phi_{total}/\phi_{direct}$
25	56	1.20
50	71	1.39
75	90	1.47
100	112	1.50
100	112	1.50
125	135	1.51
25	1200	1.00
50	1200	1.02
100	1200	1.06

Appendix G: Recommended Neutron Monitoring Procedure

The preceding research has been conducted with the intent of providing enough information to implement a routine neutron monitoring system for use in the vicinity of high-energy x ray therapy machines. In particular, an outline of a simple yet useful monitoring protocol may now be described. These procedures include an infrequent determination of the neutron spectrum with Bonner spheres and a total dose measurement made for every patient treatment session. It is recommended that a neutron spectrum measurement be made once per calendar quarter until it has been determined that the stability of the x ray machine is sufficient to allow a longer periodicity.

Neutron spectrum measurements require the use of the following items:

- a Bonner sphere set as described in the main body of this report.
- at least one set of seven gold foils with dimensions of 0.5" diameter and 0.002" thickness which have been precisely weighed and thickness determined.
- a G-M beta counter as described in the main body of this report.
- computer resources capable of executing the programs XFOIL.BAS and TEST10.FOR (XFOIL.BAS is a user-interactive version of FOIL5.BAS. TEST10.FOR is the NRL source code which implements the YOGI unfolding algorithm.)

XFOIL.BAS may be compiled and run on any IBM-PC compatible computer. TEST10.FOR is currently available only for DEC VAX machines running under the VMS operating system. Both of these codes are available from AFIT/ENP on request. A version of the YOGI algorithm for PC's is in development by the author, with no release date set. It too will be available from AFIT/ENP.

The gold foils should be exposed alone, outside the direct x ray path, one in each of the Bonner spheres (one foil will be bare). A

suitable distance from the x ray beam axis to the sphere center is one half meter. This distance is representative of the location where flux integrators should be placed during actual treatment sessions. In order to minimize counting times the x ray dose should be at least 5,000 Rads if possible. The following information must be recorded for each exposure:

- foil serial number.
- 24 hour clock times and five digit Julian dates for the start of exposure, end of exposure, start of counting, and end of counting.

The executable code derived from XFOIL.BAS is run to calculate foil saturation activity per milligram. As long as the items of information noted above are available, the program will prompt the user as required. If a foil serial number is not in the program's database the foil dimensions must be entered before the code will generate a result. XFOIL.BAS prompts for this information, if required. The foil activities thus calculated may be input to the TEST10.FOR executable for spectral deconvolution. Additional information on running the YOGI algorithm is available in the NRL reports referenced in this report. It should be noted that YOGI will refer to its results as time integrals. This is not correct when foil saturation activities are used with Sanna's response matrix. The magnitudes of the results are correct, but the units should actually be in terms of inverse seconds. This is a consequence of the way the code formats its output, not how it performs the calculations. The most useful result from YOGI is the dose rate equivalent calculation. Simple arithmetic enables the calculation of a conversion factor for flux to dose rate equivalent.

The conversion factor for flux to dose rate equivalent is used to process the data from flux integrators. At least one flux integrator should be placed on the treatment table for each patient exposure. A cadmium-difference pair must also be exposed at the same time, therefore this procedure uses three gold foils per measurement. The foils must be

accurately weighed and sized, with approximate dimensions of 1.0" diameter and 0.001" thickness. For a measurement the detectors should be near to each other, but more than ten centimeters apart (to avoid anomalous results from flux depression or scatter from the flux integrator). The detectors should all be placed as close to the patient's mid-section as possible without actually being in the direct x ray path. The same information as for Bonner spheres must be recorded. This information is used by XFOIL.BAS to calculate several quantities including the total patient dose equivalent due to neutrons.

Bibliography

1. NCRP Report No. 79. Neutron Contamination from Medical Electron Accelerators. National Council on Radiation Protection and Measurements, Bethesda, MD, 1 November 1984.

2. Walker, William F. et al. Chart of the Nuclides. General Electric Company-Nuclear Energy Operations, San Jose, CA, 1984.

3. McCall, R. C., T.M. Jenkins and E. Techilin. High Energy Photon Response of Moderated Neutron Detectors. Report SLAC-PUB-1768. Stanford Linear Accelerator Center, Stanford, CA 1976.

4. Price, William J. Nuclear Radiation Detection (Second Edition). New York: McGraw-Hill Book Company, 1964.

5. WADD-TR-61-174. AF NETF Graphite Standard Pile. Nuclear Engineering Test Facility, Directorate of Engineering Test, Aeronautical Systems Division, Air Force Systems Command, Wright-Patterson AFB, OH, March 1962.

6. Greenfield, Moses A. et al. "Measuring Flux Absolutely With Indium Foils," Nucleonics, 15(3): 57-61 (March 1957).

7. Stanford, George S. and James H. Seckinger. Thickness Corrections for Neutron-Activated Gold Foils. ANL-7545. Argonne National Laboratory, Argonne, IL, February 1969.

8. Bramblett, R. L. et al. "A New Type of Neutron Spectrometer," Nuclear Instruments and Methods, 9: 1-12 (1960).

9. Lowry, Kimberly A. and T. L. Johnson. The Effect of the Choice of Response Matrix on Unfolded Bonner Sphere Spectra. NRL Memorandum Report 5493. Naval Research Laboratory, Washington, December 1984.

10. -----. Modifications to Iterative Recursion Unfolding Algorithms and Computer Codes to Find More Appropriate Neutron Spectra. NRL Memorandum Report 5340. Naval Research Laboratory, Washington, June 1984.

11. Hughes, Donald J. Pile Neutron Research. Cambridge, MA: Addison-Wesley Publishing Company, 1953.

12. Kumar, Arun and P. S. Nagarajan. "Neutron Spectra of ^{239}Pu-Be Neutron Sources," Nuclear Instruments and Methods, 140: 175-179 (1977).

13. NCRP Report No. 38. Protection Against Neutron Radiation. National Council on Radiation Protection and Measurements, Bethesda, MD, 4 January 1971.

14. Bruninx, E. "The Measurement of Fast Neutron Flux Densities Above 0.5 MeV by a Simple Moderation Method," International Journal of Applied Radiation and Isotopes, 21: 657-666 (1970).

15. McCall, R. C., Chairman, NCRP Scientific Committee 60. Telephone Interview, 8 December 1986.

16. Ruegsegger, Donald, Director, Nuclear Medicine. Personal Interview. Miami Valley Hospital, Dayton, OH, 20 December 1986.

17. Radiation Detectors. Product Catalog. TGM Detectors, Inc., Waltham, MA, undated.

18. Farinelli, Ugo. "Interpretation of Activation Measurements," Proceedings of the Symposium on Neutron Monitoring for Radiological Protection. International Atomic Energy Agency, Vienna, 1967.

19. Price, William J. Nuclear Radiation Detection. New York: McGraw-Hill Book Company, 1959.

20. Jenkins, T. M. "Simple Recipes for Ground Scattering in Neutron Detector Calibration," Health Physics, 39: 41-47 (July 1980).

21. Sanna, R. S. Thirty One Group Response Matrices for the Multisphere Neutron Spectrometer Over the Energy Range Thermal to 400 MeV (HASL-267). Health and Safety Laboratory, Atomic Energy Commission, New York, March 1973.

22. -----. Telephone Interview, 8 December 1986.

23. Almond, Peter R. "Neutron Leakage from Current Machines," Proceedings of a Conference on Neutrons from Medical Electron Accelerators (NBS Special Publication 554). 129-138. United States Government Printing Office, Washington, 1979.

24. Anderson, M. Edward. "Increases in Neutron Yields of Plutonium-Beryllium (α,n) Sources," Nuclear Applications, 4: 142-147 (March 1968).

25. -----. "Increases in Neutron Yields of ^{239}Pu-Be (α,n) Sources-II," Nuclear Technology, 52: 428-430 (March 1981).

26. Mound Laboratory. Shipping Data-Plutonium Neutron Source. Neutron Source No M-1170. Monsanto Research Corporation, 9 March 1962.

VITA

Lieutenant Mark J. Rossano [redacted] He was graduated from high school there in 1976 and attended the United States Naval Academy, from which he received the degree of Bachelor of Science in May 1980. Upon Graduation he was commissioned in the United States Navy. He pursued professional qualification as a Surface Warfare Officer, and was so designated in December 1983. He served four years at sea, in USS Jesse L. Brown (FF-1089), and USS Iowa (BB-61) until entering the School of Engineering, Air Force Institute of Technology, in August 1985. He was reassigned to duties as Engineer Officer in USS Capodanno (FF-1093) in October 1987 after completing the six month shipboard Department Head Course at Surface Warfare Officer's School.

[redacted]

REPORT DOCUMENTATION PAGE

Form Approved
OMB No. 0704-0188

1a. REPORT SECURITY CLASSIFICATION
UNCLASSIFIED

1b. RESTRICTIVE MARKINGS

2a. SECURITY CLASSIFICATION AUTHORITY

2b. DECLASSIFICATION / DOWNGRADING SCHEDULE

3. DISTRIBUTION / AVAILABILITY OF REPORT
Approved for public release;
distribution unlimited

4. PERFORMING ORGANIZATION REPORT NUMBER(S)
AFIT/GNE/ENP/89J-1

5. MONITORING ORGANIZATION REPORT NUMBER(S)

6a. NAME OF PERFORMING ORGANIZATION
School of Engineering

6b. OFFICE SYMBOL (*If applicable*)
AFIT/ENP

7a. NAME OF MONITORING ORGANIZATION

6c. ADDRESS (*City, State, and ZIP Code*)
Air Force Institute of Technology
Wright-Patterson AFB OH 45433

7b. ADDRESS (*City, State, and ZIP Code*)

8a. NAME OF FUNDING / SPONSORING ORGANIZATION

8b. OFFICE SYMBOL (*If applicable*)

9. PROCUREMENT INSTRUMENT IDENTIFICATION NUMBER

8c. ADDRESS (*City, State, and ZIP Code*)

10. SOURCE OF FUNDING NUMBERS

PROGRAM ELEMENT NO.	PROJECT NO.	TASK NO	WORK UNIT ACCESSION NO.

11. TITLE (*Include Security Classification*)
FLUX AND SPECTRUM OF NEUTRONS GENERATED FROM 25 MV MEDICAL X-RAY THERAPY MACHINE

12. PERSONAL AUTHOR(S)
Mark J. Rossano, B.S., LT USN

13a. TYPE OF REPORT	13b. TIME COVERED	14. DATE OF REPORT (*Year, Month, Day*)	15. PAGE COUNT
MS Thesis	FROM _____ TO _____		

16. SUPPLEMENTARY NOTATION

17. COSATI CODES			18. SUBJECT TERMS (*Continue on reverse if necessary and identify by block number*)
FIELD	GROUP	SUB-GROUP	Neutron spectrometry; Photonuclear interactions; Radiation monitoring; Neutron activation

19. ABSTRACT (*Continue on reverse if necessary and identify by block number*)

Thesis Advisor: George John
Professor of Nuclear Engineering
Department of Engineering Physics

20. DISTRIBUTION / AVAILABILITY OF ABSTRACT
☒ UNCLASSIFIED/UNLIMITED ☐ SAME AS RPT ☐ DTIC USERS

21. ABSTRACT SECURITY CLASSIFICATION
UNCLASSIFIED

22a NAME OF RESPONSIBLE INDIVIDUAL
George John, Professor

22b TELEPHONE (*Include Area Code*)
(513) 255-4498

22c OFFICE SYMBOL
ENP

DD Form 1473, JUN 86 *Previous editions are obsolete.*

A procedure was developed for the routine monitoring of neutron dose absorbed by patients receiving x-ray therapy with high-energy electron accelerators. The source of the neutrons was photonuclear reactions. The detection system used to measure them is described.

Three methods are described and compared for measuring the neutron flux by activation of thin gold foils. These included the cadmium-difference method for thermal flux determination, a cadmium-clad polyethylene moderator known to have a relatively "flat" response to neutrons in the energy range of interest, and a Bonner sphere set for measuring flux and the neutron energy spectrum. Results in an actual hospital installation using a BBC 45-MeV betatron revealed whole body neutron dose rates of approximately 1.5 mrem per photon rad. Two beta counting systems were calibrated so that routine measurements of neutron dose could be estimated from foil activation data and monitored for unexpected changes.